GLOBAL CLIMATIC AND STABLE ISOTOPIC CORRELATIONS DURING THE EARLY PERMIAN (CISURALIAN)

A Senior Scholars Thesis

by

JORDAN NORET

Submitted to the Office of Undergraduate Research
Texas A&M University
in partial fulfillment of the requirements for the designation as

UNDERGRADUATE RESEARCH SCHOLAR

April 2009

Major: Geology
Environmental Geoscience

GLOBAL CLIMATIC AND STABLE ISOTOPIC CORRELATIONS DURING THE EARLY PERMIAN (CISURALIAN)

A Senior Scholars Thesis

by

JORDAN NORET

Submitted to the Office of Undergraduate Research
Texas A&M University
in partial fulfillment of the requirements for the designation as

UNDERGRADUATE RESEARCH SCHOLAR

Approved by:

Research Advisor: Ethan Grossman
Associate Dean for Undergraduate Research: Robert C. Webb

April 2009

Major: Geology
Environmental Geoscience

ABSTRACT

Global Climatic and Stable Isotopic Correlations During the Early Permian (Cisuralian). (April 2009)

Jordan Noret
Department of Geology and Geophysics
Texas A&M University

Research Advisor: Dr. Ethan Grossman
Department of Geology and Geophysics

The early Permian was an interval when cool, glaciated conditions, similar to those of the present-day, shifted to warm, non-glaciated conditions. As a result, climatological information about this time period is pertinent in studying the causes and effects of global warming. This study presents new oxygen and carbon stable isotopic data ($\delta^{18}O$ and $\delta^{13}C$, VPDB) from carefully screened, early Permian brachiopod shells from the Ural Mountains. Using cathodoluminescence (CL) microscopy, 24 specimens were determined to be well-preserved and were used for 95 stable isotopic analyses. Inter-specimen variability within each time horizon was lower than 0.5‰ and intra-specimen variability was lower than 0.2‰.

The $\delta^{18}O$ values of the specimens analyzed average between -2.2‰ and -2.7‰ through the Asselian, Sakmarian, and early Artinskian (297-283 Ma). Values then rapidly increase by 3‰ in the late Artinskian and early Kungurian (~275 Ma). The low values before the Kungurian do not suggest glacial conditions and thus disagree with the geological evidence for a glacial maximum during the Asselian. These data also disagree with the early Permian maximum and subsequent decline in $\delta^{18}O$ suggested from brachiopod shell fragments from the Usolka section in the Urals (Korte et al., 2005. Palaeogeog., Palaeoclim., Palaeoecol. 224, 333-351). However, our data are similar to those obtained from other brachiopods (Grossman et al., 2008. Palaeogeog., Palaeoclim., Palaeoecol. 268, 222-233). The cause of this discrepancy is unknown, but could be a result of differences in regional oceanographic factors, glacial/interglacial conditions, or in source material (i.e. wholly preserved shells versus shell fragments). The Artinskian-Kungurian increase in $\delta^{18}O$ from this study is evidence for the aridification of the epicontinental seas of Laurussia and possibly a return to cooler conditions.

The $\delta^{13}C$ data from the specimens discussed in this study show a gradual decrease of about 1.5‰ from the late Asselian to the Artinskian, followed by a sharp increase of about 1.5‰ in the late Artinskian. This $\delta^{13}C$ increase is not seen in previously published data from Russia or North America. Further work is required before any strong conclusions can be made on global $\delta^{13}C$ variability during the early Permian.

DEDICATION

To those who teach, inspire, and set free.

ACKNOWLEDGMENTS

I would like to thank foremost my advisor, Dr. Ethan Grossman, for giving me the opportunity to participate in primary research as an undergraduate student and for his continual advice and help throughout the duration of this project. Dr. Thomas Yancey lended his paleobiological expertise extensively during this project and Dr. Boris Chuvashov also deserves special acknowledgement for his help in collecting and identifying the specimens used, as well as his expertise in the stratigraphy of the Southern Urals. Beyond the scientific side of this project, acknowledgement is owed to Shane McGary for training me on the laboratory equipment used in preparing the specimens for analysis, to Kai Tao and Josiah Straus for their help with the mass spectrometer work, and Dr. Ray Guillemete for helping me through many of the setbacks and procedural issues that I encountered. Lacey Terrette took measurements of specimen thin-sections which were used to obtain the scales of corresponding images. Lastly, and perhaps most importantly, I am greatly indebted to my mother who read this manuscript many times, giving essential grammatical and editorial advice along the way, and to my wife, Robin, who put up with me throughout this project.

NOMENCLATURE

PL	thin-section viewed under plane light
CL	thin-section viewed under cathodoluminescence light
NL	non-luminescent specimen
SMFL	shell margin and fracture luminescence in specimen
LCBL	low contrast banded luminescence in specimen
HCBL	high contrast banded luminescence in specimen
Ma	megaannum (1 million years ago)

TABLE OF CONTENTS

LIST OF FIGURES

CHAPTER I

INTRODUCTION

The understanding of past climate change is a critical tool for studying current climate. It is crucial in determining the significance of climate trends, how much and how fast the climate has changed in the past, whether human activity has caused past or present-day change, and whether the mitigation of future change is desirable and feasible. Moreover, the conclusions of paleoclimatological studies, particularly those concerning climate conditions similar to those of the present-day, are vital for providing a sound scientific basis for environmental policy decisions.

1.1 Significance of the early Permian climate

During the early Permian (~300-270 Ma), Earth's climate shifted from one similar to the present day to one much warmer, from having abundant glaciers to having few or possibly none. This is evidenced by the widespread distribution of glacial sediments dating to the Carboniferous (>300 Ma) and early Permian, and the subsequent lack thereof soon afterwards until the Cenozoic era, more than 200 million years later (Frakes et al., 1992; Isbell et al., 2003, Fielding et al., 2008). The early Permian is therefore the most recent period in Earth history from which there is ample geologic evidence that an ice-house climate, similar to that of today, shifted to a hot-house climate.

This thesis follows the style of Palaeogeography, Palaeoclimatology, Palaeoecology.

Montañez et al. (2007) synthesized available stable isotope data from this time and used these to estimate atmospheric pCO_2. This work further demonstrated that the Permian is a good analogue for the current climate in that their isotopic measurements and model calculations suggest that CO_2 concentrations were near present-day levels (<1000 ppmV) during glacial periods, and concentrations during glacial-free periods were similar to those expected in the near future (>2000 ppmV) if fossil fuel resources are totally exhausted (Montañez et al., 2007).

By researching certain climatological and ecological aspects of the early Permian world, scientists will be able to compare a climate change that took place in the absence of human activity with a present-day climate trend, such as the one described by the Intergovernmental Panel on Climate Change (IPCC, 2007). New data, carefully screened for quality, are presented in this study to strengthen the understanding of climate change during the early Permian period.

1.2 Stable isotopes as paleoclimate proxies

Stable oxygen ($^{18}O/^{16}O$) and carbon ($^{13}C/^{12}C$) isotopic measurements of well preserved carbonate fossils can be effectively used to study past climate and carbon cycle variability. Isotopic fractionation of oxygen and carbon isotopes occurs during the water cycle, mineral precipitation in seawater, and in biological processes. Some of these fractionation processes have important global and local effects on $\delta^{18}O$ and $\delta^{13}C$ in the ocean-atmosphere system and are critical to consider in stable isotopic studies.

Variation of mean seawater $\delta^{18}O$ values over million-year time scales is dependent mainly on the volume and distribution of glaciers, but can also be affected by tectonic processes over longer time scales (10^7 years) (Shackleton and Opdyke, 1973; Railsback, 1990; Veizer et al., 1999). Higher glacial volume increases seawater $\delta^{18}O$ because glacial ice is highly depleted in ^{18}O. Where marine waters are not well circulated (e.g., epicontinental seas), seawater $\delta^{18}O$ values can be regionally affected by high evaporation rates, increasing $\delta^{18}O$, or freshwater input, decreasing $\delta^{18}O$. Some researchers (e.g., Veizer et al. 1997, 1999; Veizer and Mackenzie, 2004; Wallmann, 2001, 2004) posit that seawater $\delta^{18}O$ ($\delta^{18}O_w$) values have changed significantly during the Phanerozoic as a result of tectonic processes that drive long-term exchange of lithosphere and hydrosphere components. This hypothesis better accommodates the very low $\delta^{18}O$ values that have been obtained from early Phanerozoic (Cambrian-Devonian) marine fossils (Veizer et al., 1999). Nonetheless, this long-term trend would not have significant effect over the relatively short span of time considered in this study.

Oxygen isotope compositions from well preserved calcite also record paleotemperatures from the time of formation. As a result of thermodynamically-controlled fractionation, $\delta^{18}O$ values are higher in calcite relative to the seawater in which it was precipitated. The magnitude of this fractionation is dependent on the temperature of the environment.

Epstein et al. (1953) developed an empirical relationship between ambient water temperature and $\delta^{18}O$ values of precipitated calcite. This relationship was later confirmed by O'Neil et al. (1969) and recast by Hays and Grossman (1991):

$$T(°C) = 15.7 - 4.36(\delta^{18}O_{calcite} - \delta^{18}O_{w}) + .012(\delta^{18}O_{calcite} - \delta^{18}O_{w})^2$$

where $\delta^{18}O_{calcite}$ is the $\delta^{18}O$ value of the calcite and $\delta^{18}O_w$ is the value of the seawater. By using this relationship between temperature and $\delta^{18}O$, data from well-preserved carbonate can ultimately be used to determine the temperature of the ancient marine body in which the carbonate precipitated (Shackleton and Opdyke, 1973; Grossman, 1994). However, an uncertainty in using this method for determining paleotemperatures is that the $\delta^{18}O$ of ancient seawater ($\delta^{18}O_w$) must be known, and therefore the effect of glacial volume, freshwater input, and evaporation on $\delta^{18}O_w$ must be estimated.

With regard to carbon isotopes, $\delta^{13}C$ values record changes in the carbon cycle. These changes are mainly the result of enhanced burials of organic matter, increasing $\delta^{13}C$ values in the ocean-atmosphere system (Scholle and Arthur, 1980; Schidlowski and Aharon, 1992; Kump and Arthur, 1999). However, the release of ^{13}C-depleted volcanic CO_2 (Renne et al., 1995) and methane discharges (Dickens et al., 1997) are also possible causes of $\delta^{13}C$ variability. An important local process that influences regional variation in $\delta^{13}C$ is the circulation of ^{12}C-enriched anoxic bottom-waters of the ocean system (Knoll et al., 1996).

1.3 Early Permian $\delta^{18}O$ and $\delta^{13}C$ stratigraphy

It has been widely demonstrated that there were three major glacial periods in the late Paleozoic (e.g. Frakes et al., 1992; Isbell et al., 2003, Fielding et al., 2008), the last of which ended in the early Permian (Cisuralian), the time period on which this study focuses. Data from some low paleolatitude (Korte et al., 2005) and high paleolatitude (Korte et al., 2008) brachiopods, give evidence for an Asselian-Artinskian (295-280 Ma) decrease in $\delta^{18}O$. This is an expected trend for the end of a glacial interval as ^{18}O-depleted glacial water is returned to the oceans and is concomitant with the end of the Cisuralian glacial episode. However, some researchers (e.g., Grossman et al., 2008) contend that the conclusions from the low-latitude data require confirmation as the specimens analyzed were small shell fragments and not wholly-preserved shells. In contrast with the trend observed by Korte et al. (2005, 2008), data from Grossman et al (2008), including some from the same low latitude sites as Korte et al. (2005), show an Asselian-Artinskian *increase* in $\delta^{18}O$. These authors largely attribute the upward trend to regional aridification exacerbated by restricted circulation in the epicontinental seas that covered the specimen localities during this time.

Trends in carbon sequestration have also been used to investigate the record of climate change. Although $\delta^{13}C$ data from carbonate fossils are sparse and vary widely, Grossman et al. (2008) observed that each of the three late Paleozoic glacial events described by Isbell et al. (2003) and Fielding et al. (2008) occurred nearly concurrently with or after a rise in $\delta^{13}C$. This suggests that these glacial events were in some way related to carbon sequestration. However, inconsistencies that exist in the available data from Korte et al. (2005) and Grossman et al. (2008) (i.e., differences between Uralian and North American data) points to the difficulties in resolving a global signal for carbon system perturbations.

1.4 Significance of this study

In this study, I present new $\delta^{18}O$ and $\delta^{13}C$ data from 30 carefully screened brachiopod shells to strengthen the present understanding of the climate during the early Permian. My data are especially interesting in that the specimens used are similar in locality and age as those used by Korte et al. (2005), but wholly-preserved brachiopod shells were micro-sampled (<150 µg powders) for analysis instead of macro-sampled shell fragments (150-450 µg "splinters" and 1-3 mg aliquots) (Korte et al., 2005).

CHAPTER II

SPECIMENS AND METHODS

2.1 Specimens and specimen localities

Many marine organisms such as foraminifera, brachiopods, and bivalves precipitate accretionary hard parts such as shells that are made of calcium carbonate ($CaCO_3$) which can then be analyzed for stable oxygen and carbon isotopes. Fossil brachiopods have been shown to be especially useful for stable oxygen and carbon isotopic research (Compston, 1960). Most importantly, the thick secondary layer of contemporary brachiopod shells has been shown to precipitate at or near oxygen isotopic equilibrium with coeval seawater (e.g. Parkinson et al., 2005) and oxygen isotope data from fossil brachiopods show minimal variability between co-occurring taxa (Grossman et al., 1991; Lee and Wan, 2000). Secondly, the calcitic mineralogy, low magnesium content, and dense microstructures of the shells give them a superior resistance to diagenetic alteration (Compston, 1960; Lowenstam, 1961; Popp et al., 1986). Thick shells can be especially resistant, so that studies of seasonal variation are even possible (Mii and Grossman, 1994). For these reasons, carbon and oxygen stable isotope data from chemically-pristine brachiopod shells can be used to construct reliable stable isotope stratigraphies for sediments as old as Paleozoic.

The specimens used in this study were collected from early Permian exposures in the Southern Urals near the Russian cities of Kungur, Krasnoufimsk, and Sterlitimak

(**Figure 1**). This field work was conducted by Dr. Thomas Yancey, a professor of geology at Texas A&M University, USA, with the help of Dr. Boris Chuvashov, a geologist with the Urals Branch of the Russian Academy of Sciences. Specimens collected were assigned to stratigraphic "horizons", roughly the Russian equivalent to U.S. formations, based on the stratigraphy established by Russian stratigraphers (e.g. Chuvashov and Nairn [1993], Chuvashov and Chernykh [2000], and Chuvashov et al. [2002]). These stratigraphic horizons are primarily based on faunal zones (foraminifers, ammonoids, and conodonts) described by Chuvashov et al. (2002).

Originally, 45 brachiopod shells were selected for this study. However, 14 were excluded from analysis because they were poorly preserved or were too thin for proper isotopic analysis. This left 31 specimens: eight from the late Asselian, four from the early Sakmarian, one from the early Artinskian, two from the middle Artinskian, 11 from the late Artinskian, and five from the early Kungurian. The genera include *Chaoiella, Kalitvella*, *Purdonella*, and *Stenoscisma*. See **Figure 2** for an overview of these 31 specimens and **Appendix C** for detailed information on all of the specimens selected for this study.

Specimen paleogeography

According to Blakey (2008) and Scotese (2008), the study area was at a latitude of ~30° north during the early Permian. Laurussia was converging with the Kazakhstanian and Siberian plates – producing the Ural orogeny and shoaling the Russian Platform Seaway

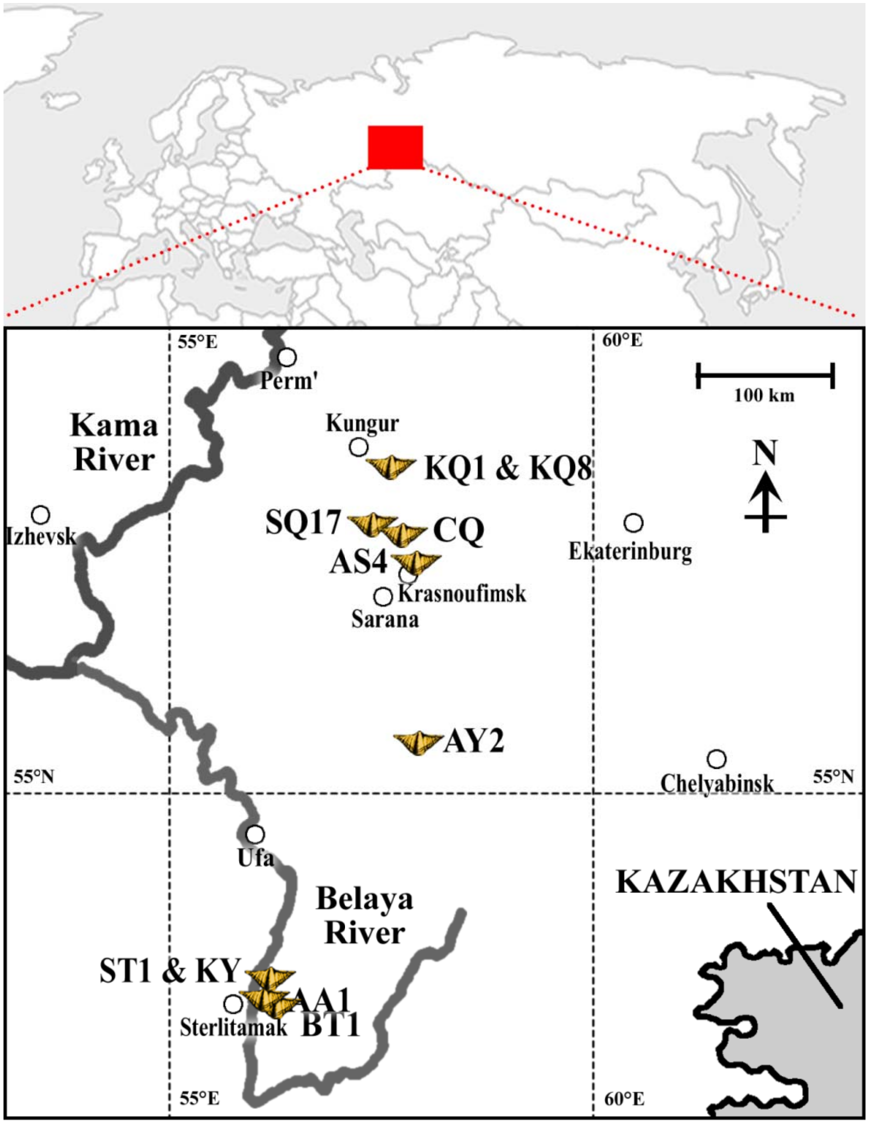

Figure 1. Specimen localities in the Southern Urals of Russia.

LEGEND

- Russia
- Kazakhstan
- specimen locality
- city or town
- river (width not to scale)
- Meridians/Parallels

Specimen ID	Latitude, Longitude
SQ17	56° 52.1'N, 57° 25.0'E
KQ8	57° 23'N, 57° 05.9'E
KQ1	57° 23'N, 57° 05.9'E
AY2	55° 22'N, 57° 59'E
CQ	56° 48.1'N, 57° 43.7'E
AS4	56° 30.3'N, 57° 41.9'E
AA1	53° 33.9'N, 56° 04.4'E
ST1	53° 44.3'N, 56° 06.1'E
KY	53° 44.3'N, 56° 06.1'E
BT1	53° 33.2'N, 56° 05.9'E

Stage	Horizon (Formation)	Locality*	Depositional Environment	Taxon	Specimen ID	Age#
Kungurian	Saraninian (Lower Saraninian Member)	Nizhneizginsk	argillaceous micrite / interreef muds	*Kalitvella sp.*	SQ17b	274.8
					SQ17a	274.8
		Chikali quarry, Kungur city	biomicrite / small 'reef' and bedded limestone	*Stensocsisma mutabilis*	KQ8-2	274.5
					KQ8-1	274.5
				Chaoiella	KQ1-1	275
Artinskian	Sarginskian	Mechetlino village	gravelly shell concentrates and poorly sorted argillaceous sands / debris flow into flysch basin (non-reef)	*Stenoscisma mutabilis*	AY2-6	275.7
				Kalitvella sp.	AY2-4b	275.7
					AY2-4a	275.7
					AY2-3	275.7
				Chaoiella	AY2-2	275.7
		Lebayshye quarry, Chatlik village	biomicrite & biosparite / small reef with abundant fossils		CQ3-1	276
				Stenoscisma mutabilis	CQ15-1	276.3
				Kalitvella sp.	CQ12-2	276.3
					CQ12-1	276.3
				Chaoiella	CQ13-2	276.5
					CQ13-1	276.5
	Irginskian	Sarana village	argillaceous micrite with shells / bedded limestone	*Chaoiella*	AS4-6	278.6
				Stenoscisma mutabilis	AS4-3	278.6
	Burzevskian	Maly tau shikhan, Sterlitamak	biomicrite & biosparite / reef massif with abundant fossils (bioherm)	*Kalitvella sp.*	AA1-1	283
Sakmarian	Tastubskian	Yurak tau shikhan, Sterlitamak	biomicrite & biosparite / reef massif with abundant fossils (bioherm)	*Purdonella nikitini*	ST1-2	293
					ST1-1	293
				Kalitvella sololovi	KY-2	293
					KY-1	293
Asselian	Shikhanskian	Tra tau shikhan, Sterlitamak	biomicrite & biosparite / reef massif with abundant fossils (bioherm)	*Stenoscisma mutabilis*	BT1-6	296
					BT1-5	296
				Chaoiella	BT1-4	296
					BT1-3	296
				Purdonella nikitini	BT1-2	296
					BT1-1	296
				Kalitvella sololovi	BT1-K2	296
					BT1-K1	296

Figure 2. Lithology and stratigraphy of the 31 specimens used in this study.
* All localities are in the Southern Urals of Russia.
\# Ages are from Gradstein et al. (2004).

that connected the Paleo-Tethys and Boreal oceans (**Figure 3**). The study area was located in this seaway, with most of the brachiopod specimens coming from the shelf margin on the west side of the Preuralian foredeep, an area characterized by shallow, nutrient-rich water, large reef systems, and bioherms (Chuvashov and Nairn, 1993). These reefs and bioherms first began to grow in the Asselian and mark the geographic transition zone between shallow seas covering the eastern margins of the Russian craton and the deeper seas of the Preuralian foredeep (Chuvashov and Nairn, 1993). Many of the specimens chosen for this study were collected from Tra tau shikhan, Yurak tau shikhan, and Maly tau shikhan, which are examples of these large bioherms (**Figure 4**). Most of the specimen lithologies are dominated by biomicrites, biosparites, or argillaceous micrites, suggestive of a reef environment. The five AY specimens were taken from gravelly shell concentrates and poorly sorted argillaceous sands indicative of deposition by a debris flow that originated on the east margin of the Preuralian foredeep.

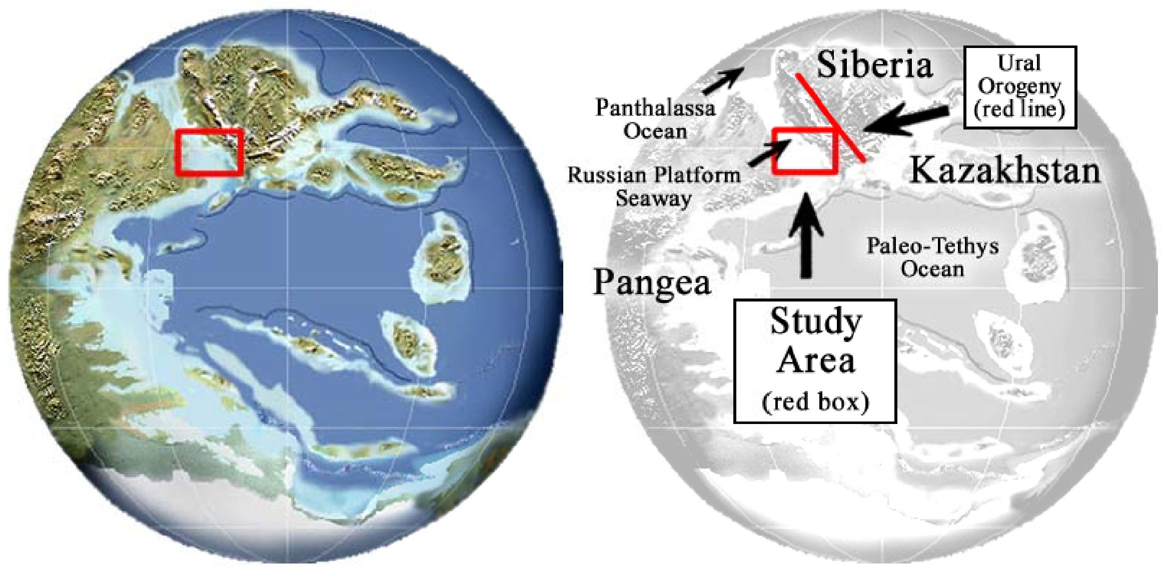

Figure 3. Paleogeography of Permian period (270 Ma) showing the study area. Modified from Blakey (2008).

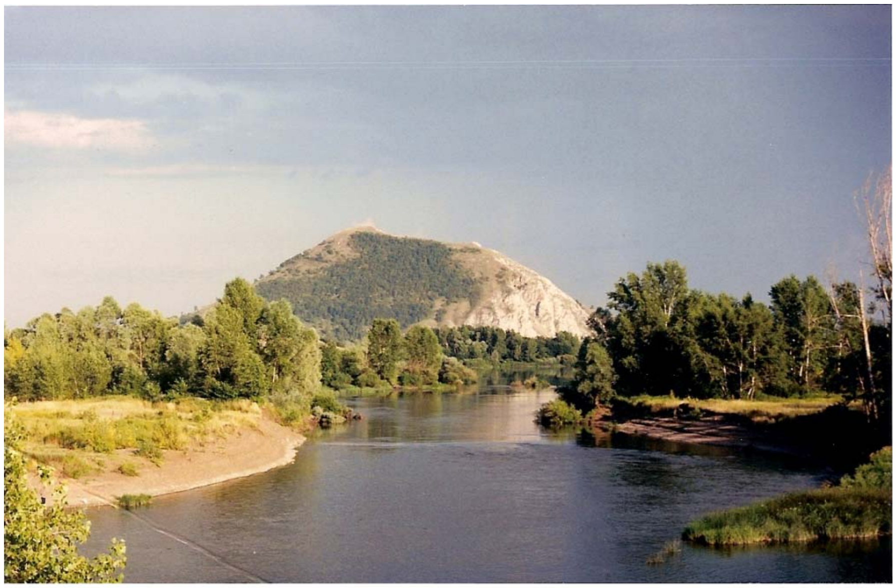

Figure 4. Photo of Yurak Tau shikhan (background) near Sterlitamak, Russia; *courtesy of Ethan L. Grossman.* This is an example of the immense bioherms (shikhans) from which the Asselian, Sakmarian, and early Artinskian specimens used in this study were collected.

2.2 Methods

First, brachiopod specimens were obtained and identified to genus and species, if possible. Specimens were embedded in epoxy and cut longitudinally in preparation for making thin sections. The plane of thin section was determined to take advantage of the thickest part of each shell when sampling the resulting billets. To acquire isotopic data most representative of original shell chemistry, I used a slightly modified version of the "TAMU" method described by Grossman (1994) and Mii et al. (1999, 2001) for checking specimen preservation. This method is itself a modification of the method first used by Popp et al. (1986) who used cathodoluminescence (CL) microscopy to determine manganese (Mn) content of thick-sectioned shells, as increasing Mn content causes brighter luminescence. Increased Mn content is indicative of post-deposition alteration and is thus used as an indicator for diagenetic influence (Popp et al., 1986; Grossman, 1994). This technique was extended in the TAMU method by going a step further and producing and photographing thin sections under plane-polarized light (PL) and CL. Shells that are characterized as luminescent under CL or as opaque, dark, or cloudy under PL were avoided for isotopic analysis. This CL microscopy technique was demonstrated by Bruckschen et al. (1999), as discussed by Grossman et al. (2008), to be more effective at reducing the contamination by secondary calcite than the "Ruhr" method used by Veizer et al. (1999), Bruckschen et al. (1999), and Korte et al. (2005, 2008).

Specifically, I used a TECHNOSYN Model 8200 MK II cathodoluminescence stage to obtain PL and CL photographs of my specimens. The physical preservation of each was checked using the PL photographs. Each shell that displayed a prismatic or fibrous microstructure was characterized as "preserved" and the rest as "not preserved". The degree of luminescence in each specimen was characterized using a slightly modified version of the scheme used in the TAMU method. Shells that were dominantly non-luminescent were labeled as "non-luminescent" (NL; **Figure 5A**). Shells that only displayed luminescence along shell margins and fractures were labeled as "shell margin and fracture luminescent" (SMFL; **Figure 5B**). Shells that displayed alternating bands of luminescence and non-luminescence were labeled as "high-contrast banded luminescent" (HCBL; **Figure 5C**) while shells that displayed alternating bands of bright and dull luminescence were labeled as "low-contrast banded luminescent" (LCBL;

Figure 5D). Shells that were dominantly luminescent were labeled as "luminescent" (L). **Figure 5** shows examples of LCBL, HCBL, SMFL, and NL shells. However, this method is still not fool-proof for identifying diagenetic alteration. For example, Barbin and Gaspard (1995) showed that parts of unaltered modern brachiopod shells display luminescence while Rush and Chafetz (1990) and Qing and Veizer (1994) showed that some altered fossil shells are non-luminescent.

Using these PL and CL images as a reference (**Appendix B**), only non-luminescent areas of each specimen were sampled with a dental drill using a 500 µm stainless-steel bur. I sampled each specimen as many times as possible, ranging from one to eight areas (average ~ four), to best provide a seasonally averaged value for the whole specimen. This sampling technique also reduces the chance of skewed data that would result if part of the specimen is chemically altered, or if slight contamination from the matrix or epoxy occurred in one of the sampling sites. When possible, I also sampled the rock matrix surrounding each specimen. Approximately 300-500 µg of powder was extracted from each sampling site and was stored in a labeled micro-centrifuge tube and analyzed separately. About 150±50 µg of each powder sample was then digested in concentrated phosphoric acid (specific gravity = 1.91-1.93) on a ThermoFinnigan Gas Bench II device. The CO_2 released was analyzed on a ThermoFinnigan DeltaPlusXP isotope ratio mass spectrometer at the Geology and Geophysics Stable Isotope Laboratory, Texas A&M University (TAMU).

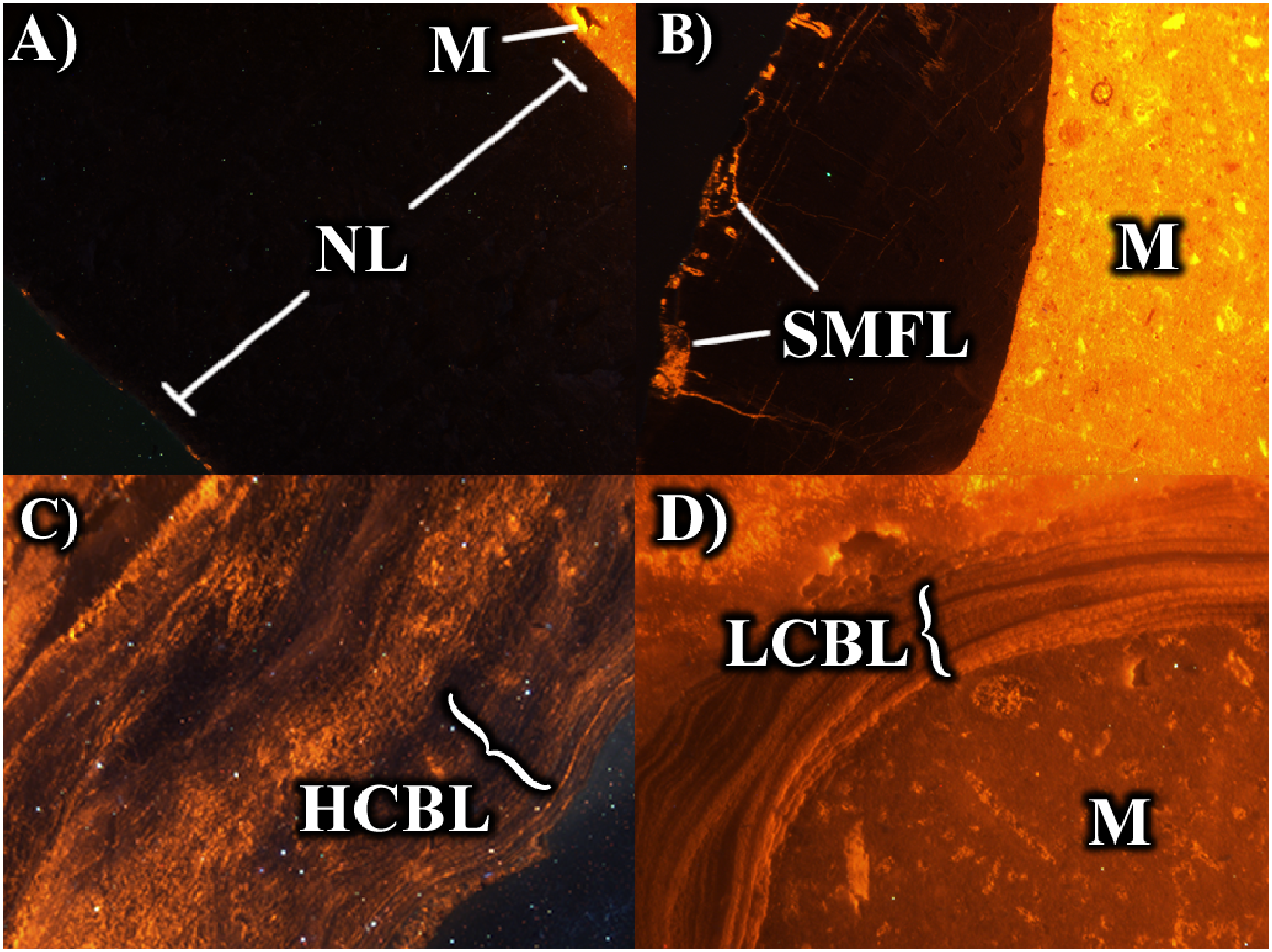

Figure 5. CL characterization classes as described in the text: A) **NL** or non-luminescent, B) SMF**L** or shell margin and fracture luminescence, C) HCBL or high-contrast banded luminescence, and D) LCBL or low-contrast banded luminescence. M = Matrix. See **Appendix B** for all CL/PL images.

Stable isotope data are reported using delta (δ) notation which compares the relative abundances of minor and major isotopes in a sample, such as $^{18}O/^{16}O$ or $^{13}C/^{12}C$ in carbonate, to those of an established standard:

$$\delta\ (‰) = ([R_{sample} / R_{standard}] - 1) * 1000$$

where R (ratio) = (abundance of minor isotope / abundance of major isotope)

The data reported herein were calibrated to the Vienna Pee Dee Belemnite (VPDB) standard using NBS-19 reference material ($\delta^{13}C$ = 1.95‰, $\delta^{18}O$ = -2.20‰). As an in-house check for the TAMU stable isotope laboratory, one NBS-19 sample is analyzed at the start and end of each 9-sample run. Analytical precision, the standard deviation (1σ) of replicate analyses of the NBS-19 standard, averaged ±0.09‰ for $\delta^{18}O$ and ±0.05‰ for $\delta^{13}C$ (**Appendix C**). The full procedure used in this study appears in **Appendix A**.

CHAPTER III

RESULTS AND DISCUSSION

3.1 Specimen quality

Of the 31 specimens examined under plane light (PL), all but one (CQ3-1) were determined to have preserved microstructure (**Figure 6**). Using CL microscopy, 12 of the specimens were determined to be almost completely devoid of a luminescent texture and were thus labeled as NL. Twelve were dominantly non-luminescent but displayed some luminescent areas along shell margins and fractures, and were labeled as SMFL. Six specimens displayed a luminescent banding texture (four LCBL and two HCBL), and CQ3-1 was completely luminescent (L). This luminescent specimen was not analyzed for isotopic data. CQ3-1 and all six of the shells which displayed banded luminescence are *Chaoiella*. Considering that the shells of this genus are characterized by a thick layer of coarsely fibrous calcite, a structure that is seldom found in productoid brachiopods, it seems likely that this shell microstructure is linked to banded luminescence. Similar banding in fossil cephalopods is believed to be caused by seasonality, stress, and periods of slow growth (Barbin et al., 1995).

3.2 Data and observed trends

For this study, 95 samples from the 24 NL and SMFL specimens were isotopically analyzed (**Figures 6 and 7**). Considering their luminescent quality, these specimens are believed to provide the most representative data for coeval seawater conditions. The six specimens with luminescent banding were also analyzed to better understand the nature of this banding. Co-occurring matrix was also sampled and analyzed, when possible.

Variability

In order to discern the significance of possible temporal trends in stable isotopic data, it is of utmost importance to measure the variability within each specimen and between specimens of similar age. Specimens were sampled serially as many times as practical from the anterior end to the dorsal end, and especially thick shells were also sampled serially from the outer margin to the inner margin. The mean intra-specimen variability (1σ) for specimens with more than one sampled area was calculated to be ±0.2‰ ($\delta^{18}O$) and ±0.1‰ ($\delta^{13}C$) for NL and SMFL specimens, and ±0.3‰ ($\delta^{18}O$ and $\delta^{13}C$) for HCBL and LCBL specimens. This low intra-sample variation suggests that the data is not skewed by poor sampling methods (e.g., sampling inconsistencies) or sample contamination (e.g., from matrix or altered shell), and that the data is representative of the true values of the fossil shells. It is also indicative that seasonality changes were only on the order of ±0.1-0.3‰.

Stage	Specimen ID	Age#	PL	CL	N	δ13C AVG (NL/SMFL)	δ13C STD (NL/SMFL)	δ18O AVG (NL/SMFL)	δ18O STD (NL/SMFL)	δ13C AVG (LCBL/HCBL)	δ13C STD (LCBL/HCBL)	δ18O AVG (LCBL/HCBL)	δ18O STD (LCBL/HCBL)	N	δ13C AVG Matrix	δ13C STD Matrix	δ18O AVG Matrix	δ18O STD Matrix
Kungurian	SQ17b	274.8	P	SMFL	2	5.88	0.16	-0.86	0.33					1	2.56		-2.39	
	SQ17a	274.8	P	SMFL	3	5.47	0.18	-0.99	0.33									
	KQ8-2	274.5	P	SMFL	1	5.84		0.25						1	5.57		-3.60	
	KQ8-1	274.5	P	NL	2	6.02	0.11	0.44	0.02					1	5.34		-3.26	
	KQ1-1	274.5	P	LCBL	3					4.78	0.44	-2.18	0.60	1	6.00		-3.87	
Artinskian	AY2-6	275.7	P	SMFL	3	6.11	0.38	-0.45	0.91					2	1.94	0.07	-4.09	-5.43
	AY2-4b	275.7	P	SMFL	2	6.16	0.01	-1.27	0.00					2	5.57	0.07	5.57	0.07
	AY2-4a	275.7	P	SMFL	3	5.41	0.13	-1.64	0.05									
	AY2-3	275.7	P	SMFL	3	5.93	0.33	-0.18	0.07					2	-0.12	0.37	-5.80	0.13
	AY2-2	275.7	P	HCBL	3					4.65	0.20	-3.14	0.21					
	CQ3-1	276	NP	L	NOT ANALYZED													
	CQ15-1	276.3	P	NL	3	5.17	0.12	-2.23	0.16					1	5.24		-2.05	
	CQ12-2	276.3	P	SMFL	4	6.01	0.13	-2.25	0.09					1	5.25		-2.35	
	CQ12-1	276.3	P	SMFL	3	5.76	0.11	-2.05	0.03					1	5.17		-1.63	
	CQ13-2	276.5	P	HCBL	6					4.26	0.38	-2.25	0.12					
	CQ13-1	276.5	P	NL	4	4.79	0.06	-2.16	0.05					1	3.08		-4.16	
	AS4-6	278.6	P	LCBL	4					3.29	0.30	-3.22	0.13	1	2.94		-4.75	
	AS4-3	278.6	P	SMFL	3	4.32	0.09	-2.90	0.12					1	2.75		-5.12	
	AA1-1	283	P	NL	6	4.68	0.09	-2.17	0.10					2	3.65	0.18	-3.05	0.35
Sakmarian	ST1-2	293	P	NL	5	5.04	0.06	-2.80	0.05					1	4.89		-1.20	
	ST1-1	293	P	SMFL	6	4.59	0.12	-2.69	0.16					2	5.10	0.03	-1.33	0.05
	KY-2	293	P	NL	8	5.68	0.05	-2.60	0.12					2	4.99	0.03	-0.87	0.04
	KY-1	293	P	NL	6	4.50	0.07	-2.51	0.12					1	5.04		-0.81	
Asselian	BT1-6	296	P	NL	1	5.55	0.00	-2.32	0.00					1	5.58		-1.98	
	BT1-5	296	P	NL	5	6.35	0.13	-2.26	0.08					2	5.89	0.15	-1.30	0.30
	BT1-4	296	P	LCBL	4					3.26	0.09	-2.26	0.11	1	5.55		-1.63	
	BT1-3	296	P	LCBL	2					3.67	0.47	-2.40	0.40	1	5.76		-1.08	
	BT1-2	296	P	NL	6	6.20	0.18	-2.65	0.15									
	BT1-1	296	P	NL	5	5.66	0.13	-2.86	0.13					1	5.66		-1.84	
	BT1-K2	296	P	NL	3	5.67	0.21	-2.20	0.15					1	5.78		-1.29	
	BT1-K1	296	P	NL	8	5.65	0.13	-3.38	0.42					2	5.51	0.02	-3.77	0.35

Figure 6. Specimen quality and data summary. See **Appendix C** for more detailed version.
P = Preserved; NP = Not preserved; see text for CL characterization scheme (NL, SMFL, LCBL, and HCBL)
N = # of samples analyzed from specimen; AVG = mean; STD = standard deviation (1σ)
# Ages are from Gradstein et al. (2004).

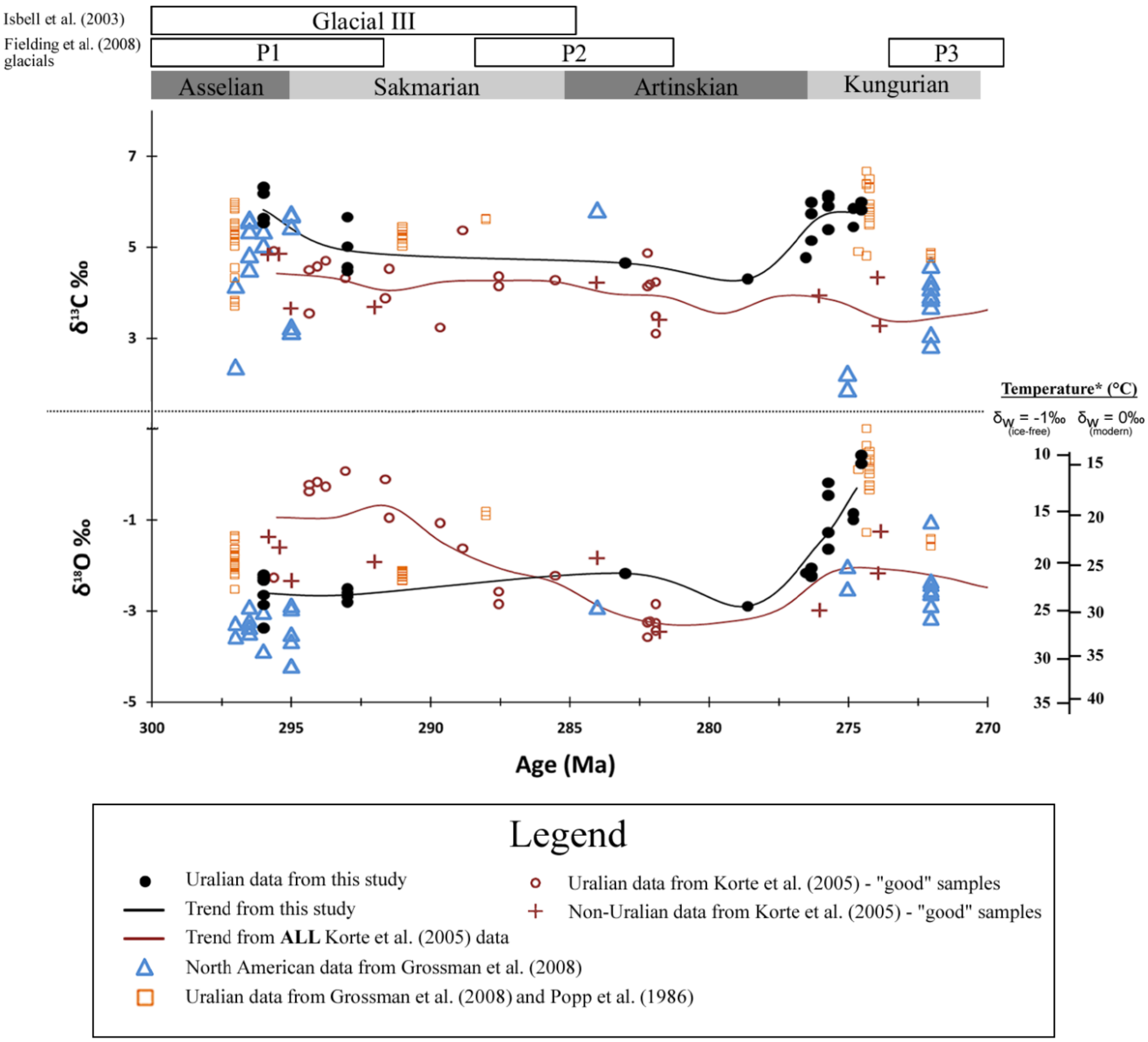

Figure 7. Oxygen and carbon isotopic compositions of 24 NL and SMFL brachiopod specimens versus age. Data includes those provided by this study (NL and SMFL shell data only), Popp (1986), Korte et al. (2005), and Grossman et al. (2008). Data trends are given for Uralian data from this study and Korte et al. (2005).

*Temperatures were calculated using the equation reported in Hays and Grossman (1991) modified from O'Neil et al. (1969).

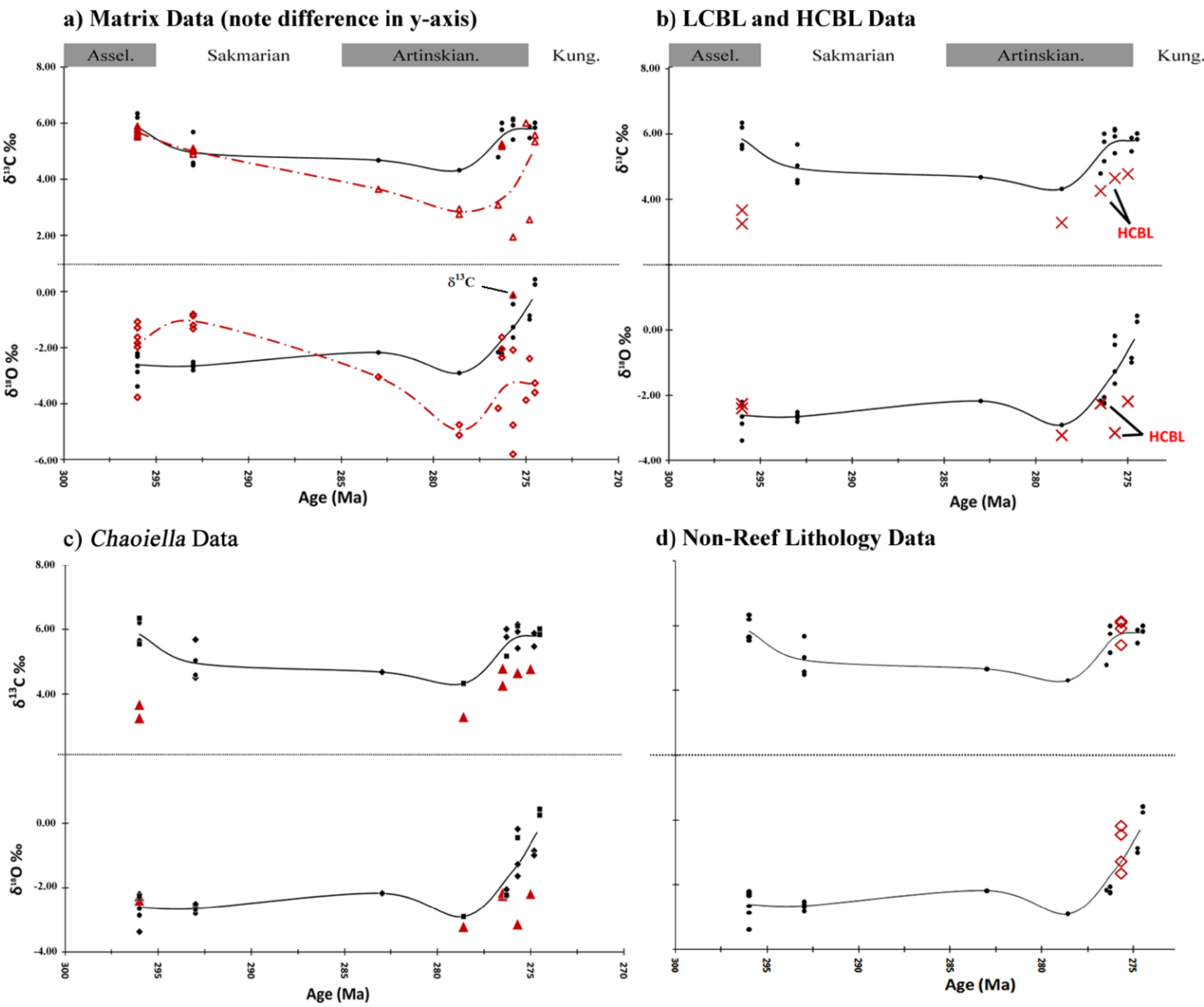

Figure 8. Oxygen and carbon isotopic data differentiated by sample material, luminescence character, brachiopod taxonomy, and lithology. A) Matrix data compared to shell data. B) Data from the 6 LCBL/HCBL specimens compared to the NL/SMFL specimens. C) *Chaoiella* data compared to other genera, and D) Non-reef lithology data compared with reef lithology data.

Means were calculated for each geologic horizon (See Appendix C7 and C9) which were used to construct the trend lines.

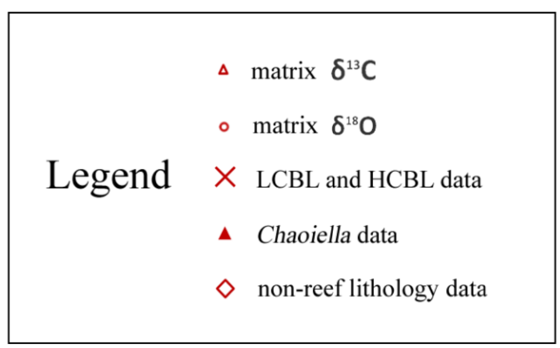

Inter-specimen variability (1σ) between NL and SMFL specimens within each stratigraphic horizon was also calculated (representing the variation between specimens of similar age), which averaged ±0.5‰ for $\delta^{18}O$ and ±0.4‰ for $\delta^{13}C$. Inter-specimen variability was not calculated for HCBL or LCBL specimens as there were too few from within similar stratigraphic horizons; therefore variability between these specimens would have been dominated by temporal variation. Although it is small, it is important to consider this magnitude of variation when comparing data temporally or geographically, as differences smaller than the inter-sample variability would not have any significance.

To test if any significant variation existed between specimens from reef deposits and those from non-reef deposits of similar age, the Mechetlino (non-reef lithology) data were plotted separately (**Figure 8d**). Although inter-specimen variability was higher in the Mechetlino (non-reef) specimens, the average values did not extend above or below those of the slightly older specimens (Chatlik) or the slightly younger specimens (Kungur and Nizhneizginsk). For these reasons, the Mechetlino data will not be discussed independently of the reef deposit data.

Oxygen isotope record

In general, the $\delta^{18}O$ data for the NL and SMFL specimens show relatively constant values in the late Asselian (~296 Ma), Sakmarian (~293 Ma), and into the late Artinskian (~276.3 Ma) (**Figures 6 and 7**). The specimens from this interval are from shikhan bioherms near Sterlitimak described in Chapter II. A mean $\delta^{18}O$ value of -2.6 ± 0.5‰ (N=6) from late Asselian specimens remains unchanged in the early Sakmarian specimens averaging -2.7 ± 0.1‰ (N=4). This increased slightly to a $\delta^{18}O$ value of -2.2‰ (N=1) for the early Artinskian specimen and then decreased again to -2.9‰ for the middle Artinskian specimen (N=1). However, only one specimen each was analyzed for the early and middle Artinskian and therefore the data may not be sufficiently representative of this time interval. There are two datasets for the late Artinskian: specimens from Chatlik (~276.3 Ma; reef lithology) show an increase in $\delta^{18}O$ to -2.2 ± 0.1‰ (N=4) and specimens from Mechetlino (~275.7 Ma; non-reef lithology) also show an increase to a mean of -0.9 ± 0.7‰ (N=4). This increasing trend continued into the early Kungurian; the specimens from Kungur and Nizhneizginsk average -0.3 ± 0.7‰ (N=4).

Of the six HCBL and LCBL specimens, three have similar $\delta^{18}O$ values compared with the NL and SMFL specimens and three have lower values (**Figures 6 and 8a**). Two specimens (one LCBL shell from the Kungurian, and one HCBL shell from the late Artinskian) have values that are ~2‰ lower than co-occurring taxa from this study. A third specimen (an LCBL shell from the late Artinskian) has a slightly lower (~0.3‰) $\delta^{18}O$ value from the other specimen of the same age. The remaining HCBL and LCBL specimens fall within a similar range of values acquired from the NL and SMFL specimens of similar age. As a result, the differences in $\delta^{18}O$ appear to not be correlative with whether the shell displays an LCBL or HCBL texture. However, when also considering the slightly higher intra-specimen variability that exists in the LCBL and HCBL specimens, future studies using specimens with banded luminescence should use greater scrutiny in specimen screening and sampling.

Carbon isotope record

The $\delta^{13}C$ data from the NL and SMFL specimens show a gradual decrease from the late Asselian (~295 Ma) mean $\delta^{13}C$ value of 5.9 ± 0.3‰ (N=6) to a mean of 5.0 ± 0.5‰ (N=4) in the early Sakmarian specimens (**Figures 6 and 7**). This decreasing trend continued with a mean of 4.7‰ in the early Artinskian (N=1) and 4.3‰ in the middle Artinskian (N=1). There are two $\delta^{13}C$ datasets for the late Artinskian: specimens from Chatlik show an increase to 5.4 ± 0.6‰ (N=4) and specimens from Mechetlino also show an increase to a mean of 5.9 ± 0.3‰ (N=4). This increasing trend appears to level off in the early Kungurian; the specimens from Kungur and Nizhneizginsk have a mean $\delta^{13}C$ value of 5.8 ± 0.2‰ (N=4).

The carbon isotope data acquired from the six HCBL and LCBL specimens show an interesting trend (**Figures 6 and 8b**). All six give much lower $\delta^{13}C$ values than co-occurring specimens from this study. Data from the two late Asselian shells are ~2.5‰ lower while the remaining four shells are ~1‰ lower. It appears that these differences in $\delta^{13}C$ values are not correlative with the banding texture and are more likely related to biological processes, considering all six specimens belong to the genus *Chaoiella*. This suggests that this genus preferentially incorporates ^{12}C relative to the other brachiopods analyzed. Such taxon-dependent vital effects have been previously suggested in other brachiopods (e.g., Popp et al., 1986; Mii et al., 2001).

Matrix data

On average, matrix $\delta^{18}O$ values are higher than those in co-occurring shells by about 1.5‰ for the Asselian and Sakmarian (**Figures 6 and 8b**). This ^{18}O enrichment in matrix relative to shell is unlike most previously published data (e.g., Mii et al., 1999) with the exception of some Moscovian samples from the Moscow Basin (Mii et al., 2001). Matrix $\delta^{18}O$ values are lower than those of co-occurring shells in the Artinskian and Kungurian specimens. The cause of this transition is interesting and remains to be elucidated. Average matrix $\delta^{13}C$ values from each locality are consistently lower than co-occurring shells, as expected, and follow a trend similar to the shell data, except for the late Artinskian and Kungurian specimens, for which matrix $\delta^{13}C$ values become highly variable (**Figures 6 and 8b**).

3.3 Discussion

Korte et al. (2005) published $\delta^{18}O$ data from some Uralian brachiopods that show very high values (above -1‰) during the Asselian. However, those from this study, as well as from data published by Grossman et al. (2008) from Uralian and North American brachiopods are much lower, averaging below -2‰ (**Figure 7**). Furthermore, the Uralian data published by Korte et al. (2005) indicate a decrease of more than 2‰ in

$\delta^{18}O$ from the Asselian to the Artinskian (295-280 Ma), while the data from this study are relatively constant for the Asselian and Sakmarian (295-290 Ma). In this study, all ten specimens analyzed from this interval were well-preserved and collected from the shikhan bioherms near Sterlitimak. Considering the likely pristine nature of these shells, it is very possible that the high glacial volume during the Asselian (Isbell et al., 2003; Fielding et al., 2008) did not have a significant impact on $\delta^{18}O_w$ in the Laurussian epicontinental seas where my specimens originated. Although this disagrees with the high Asselian and Sakmarian $\delta^{18}O$ values reported by Korte et al. (2005), their data were reportedly taken from brachiopod shell fragments, not wholly-preserved shells, which may be a cause of the anomalous $\delta^{18}O$ records. Another possibility is that the data from this study represent interglacial conditions, while those of Korte et al. (2005) represent glacial conditions. To clarify these results and make stronger conclusions regarding Asselian and Sakmarian changes in $\delta^{18}O$, further work is necessary.

Despite the discrepancy in the Asselian and Sakmarian data, the early and middle Artinskian $\delta^{18}O$ data from this study generally agree with those previously published (e.g., Korte et al., 2005; Grossman et al., 2008) (**Figure 7**). However, the late Artinskian data from this study show a more dramatic increase in $\delta^{18}O$ than these previous studies: values increased by 2‰ to 3‰ in less than five million years during the Artinskian and Kungurian. This would correlate to a drop in average ocean temperatures of more than 10°C if caused by a cooling climate and increased glacial volume, but the evidence for the onset of glaciation exists later in the Kungurian (Fielding et al., 2008). Therefore, these high values are more likely a result of the effect that regional aridification could have had on $\delta^{18}O_w$. Evaporite deposits are common in Kungurian sediments of the Ural Mountains, as reported by Chuvashov and Chernykh (2000), which suggests that this is likely the case.

The $\delta^{13}C$ data from this study do not agree with those from brachiopods previously studied by Grossman et al. (2008) and Korte et al. (2005) (**Figure 7**). Asselian and Sakmarian data from this study are about 1‰ higher than those of Korte et al. (2005) and show a decreasing trend while previous data are relatively constant during this time. Furthermore, $\delta^{13}C$ data from this study sharply increase in the late Artinskian attaining values that are more than 2‰ higher than those of North American brachiopods of similar age (Grossman et al., 2008). These differences make it difficult to interpret temporal trends in $\delta^{13}C$ during early Permian. However, considering that values are relatively constant during most of this interval, it appears that no global carbon cycle perturbations arose during this time. Variability among the data is more likely a product of regional differences in ocean circulation.

CHAPTER IV

SUMMARY AND CONCLUSIONS

I have presented data from 24 well-preserved brachiopod specimens from Russian Platform of the early Permian, along with six specimens that displayed banded luminescence, and more than 20 matrix analyses. Matrix $\delta^{13}C$ data was consistently lower than shells of the same age, as expected, while $\delta^{18}O$ values were higher in the matrix during the Asselian and early Sakmarian, after which matrix values were lower. No explanation for this $\delta^{18}O$ trend is postulated. Significant differences were not apparent in $\delta^{18}O$ and $\delta^{13}C$ values between specimens from reef and non-reef deposits. All of the *Chaoiella* specimens have lower $\delta^{13}C$ values than other co-occurring taxa, and all of the specimens with a luminescent texture were *Chaoiella*. This suggests that vital effects in *Chaoiella* play a role in both isotopic chemistry and luminescent characteristics.

$\delta^{18}O$ values of Asselian through Sakmarian data are not consistent with the decreasing trend reported from other Uralian data (Korte et al., 2005). These latter data were obtained from shell fragments, not wholly-preserved shells, which may account for this difference. The low values presented in this study, along with those already published by Grossman et al. (2008), give evidence for the possibility that the early Permian deglaciation event was not recorded in epicontinental sea brachiopods. This suggests that the high glacial volume during the Asselian (Isbell et al., 2003; Fielding et al., 2008) had little effect on $\delta^{18}O_w$ in the Laurussian epicontinental seas. However, a second possibility is that these low $\delta^{18}O$ values are representative of sea level highstands during interglacial conditions, while the high values reported by Korte et al. (2005) represent sea level lowstands during glacial conditions.

The increasing trend in $\delta^{18}O$ from the Artinskian through Kungurian in this study is consistent with other studies, and might suggest a return to cooler, possibly glaciated, conditions (e.g., Korte et al., 2005, 2008; Grossman et al., 2008). However, considering that the geologic evidence for the onset of glaciation exists later in the Kungurian, these high $\delta^{18}O$ values are more likely the product of increasingly arid conditions on the continents surrounding the Laurussian epicontinental seas. This is supported by Kungurian evaporite deposits that are common in the vicinity of the Ural Mountains (Chuvashov and Chernykh, 2000).

Finally, the $\delta^{13}C$ data from this study vary both from other Uralian brachiopod data (Grossman et al., 2008; Korte et al., 2005) and North American data (Grossman et al., 2008). This gives evidence to the probable dominance of local carbon cycle variability over global variability during the early Permian. However, further work to explicate the discrepancies between these data should be a priority if stable isotopes are to be used as paleoclimate proxies.

REFERENCES

Barbin, V., and Gaspard, D., 1995. Cathodoluminescence of recent articulate brachiopod shells. Implications for growth stages and diagenesis evaluation. Geobios, Mem. Spec., 18, 39– 45.

Barbin, V., Brand, U., Hewitt, R., and Ramseyer, K., 1995. Similarity in cephalopod shell biogeochemistry since Carboniferous: evidence from cathodoluminescence. Geobios, 28 (6), 701–710.

Blakey, R. C., 2008. Global paleogeographic views of earth history - late Precambrian to recent. http://jan.ucc.nau.edu/~rcb7/globaltext2.html.

Bruckschen, P., Oesmann, S., and Veizer, J., 1999. Isotope stratigraphy of the European Carboniferous. Proxy signals for ocean chemistry, climate, and tectonics. Chem. Geol., 161, 127-163.

Chuvashov, B.I., and Chernykh, V.V., 2000. The Kungurian age in the general stratigraphic scale of the Permian system. Doklady Earth Sciences, 375 (9), 1345-1349.

Chuvashov, B.I., Chernykh, V.V., and Bogoslovskaya, M.F., 2002. Biostratigraphic characteristic of state statotypes of the Permian system. Stratigraphy and Geological Correlation, 10 (4), 317-333.

Chuvashov, B.I., and Nairn, A.E.M., eds., 1993. Permian system: guides to geological excursions in the Uralian type localities. Occasional Publications ESRI (Earth Sciences and Resources Institute), New Series, no. 10.

Compston, W., 1960. The carbon isotopic compositions of certain marine invertebrates and coals from the Australian Permian. Geochim. Cosmochim. Acta, 18, 1 – 22.

Dickens, G.R., Castillo, M.M., and Walker, J.C.G., 1997. A blast of gas in the latest Paleocene: simulating first-order effects of massive dissociation of oceanic methane hydrate. Geology, 25, 259– 262.

Epstein, S., Buchsbaum, R., Lowenstam, H.A., and Urey, H.C., 1953. Revised carbonate–water isotopic temperature scale. Geol. Soc. Amer. Bull., 64, 1315–1326.

Fielding, C.R., Frank, T.D., Birgenheier, L.P., Rygel, M.C., Jones, A.T., Roberts, J., 2008. Stratigraphic imprint of the Late Palaeozoic Ice Age in eastern Australia: a record of alternating glacial and non-glacial climate regime. Jour. Geol. Soc. London, 165, 129–140.

Frakes, L.A., Francis, J.E., and Syktus, J.I., 1992. Climate modes of the Phanerozoic: the history of the Earth's climate over the past 600 million years. Cambridge University Press, Cambridge, Great Britain.

Gradstein, F.M., Ogg, J.G., Smith, A.G., Agterberg, F.P., Bleeker, W., Cooper, R.A., Davydov, V., Gibbard, P., Hinnov, L.A., House, M.R., Lourens, L., Luterbacher, H.P., McArthur, J., Melchin, M.J., Robb, L.J., Shergold, J., Villeneuve, M., Wardlaw, B.R., Ali, J., Brinkhuis, H., Hilgen, F.J., Hooker, J., Howarth, R.J., Knoll, A.H., Laskar, J., Monechi, S., Plumb, K.A., Powell, J., Raffi, I., Röhl, U., Sadler, P., Sanfilippo, A., Schmitz, B., Shackleton, N.J., Shields, G.A., Strauss, H., Van Dam, J., van Kolfschoten, T., Veizer, J., and Wilson, D., 2004. A Geologic Time Scale 2004. Cambridge Univ. Press, Cambridge.

Grossman, E. L., 1994. The carbon and oxygen isotope record during the evolution of Pangea: Carboniferous to Triassic. Special Paper 288, Pangea: Paleoclimate, tectonics, and sedimentation during accretion, zenith, and breakup of a supercontinent, G.D. Klein (Ed.), pp. 207-228. Boulder, Colorado, Geological Society of America.

Grossman, E. L., Yancey, T. E., Jones, T., Bruckschen, P., Chuvashov, B., Mazzullo, S., and Mii, H-S., 2008. Glaciation, aridification, and carbon sequestration in the Permo-Carboniferous: the isotopic record for low latitudes. Palaeogeog., Palaeoclim., Palaeoecol., 268, 222-233.

Grossman, E.L., Zhang, C., Yancey, T.E., 1991. Stable-isotope stratigraphy of brachiopods from Pennsylvanian shales in Texas. Geol. Soc. Amer. Bull., 103, 953–965.

Hays, P. D., and Grossman, E. L., 1991. Oxygen isotopes in meteoric calcite cements as indicators of continental paleoclimate. Geology, 19, 441– 444.

Intergovernmental Panel on Climate Change (IPCC), 2007. IPCC Fourth Assessment Report: Working Group I Report "The Physical Science Basis". Available online at http://www.ipcc.ch/ipccreports/ar4-wg1.htm.

Isbell, J.L., Miller, M.F., Wolfe, K.L., and Lenaker, P.A., 2003. Timing of late Paleozoic glaciation in Gondwana: was glaciation responsible for the development of northern hemisphere cyclothems? In: Chan, M.A., and Archer, A.W. (Eds.), Extreme depositional environments: Mega end members in geologic time, pp.5-24. Boulder, Colorado, Geological Society of America Special Paper, 370.

Knoll, A.H., Bambach, R.K., Canfield, D.E., and Grotzinger, J.P., 1996. Comparative Earth history and late Permian mass extinction. Science, 273, 452–457.

Korte, K., Jasper, T., Kozur, T. J., and Veizer, J., 2005. $\delta^{18}O$ and $\delta^{13}C$ of Permian brachiopods: a record of seawater evolution and continental glaciation. Palaeogeography, Palaeoclimatology, Palaeoecology, 224, 333-351.

Korte, K., Jones, P., Brand, U., Mertmann, D., and Veizer, J., 2008. Oxygen isotope values from high-latitudes: clues for Permian sea-surface temperature gradients and Late Palaeozoic deglaciation. Palaeogeography, Palaeoclimatology, Palaeoecology, 269, 1-16.

Kump, L.R., and Arthur, M.A., 1999. Interpreting carbon-isotope excursions: carbonates and organic matter. Chemical Geology, 161, 181–198.

Lee, X-Q., and Wan, G-J., 2000. No vital effect on $\delta^{18}O$ and $\delta^{13}C$ values of fossil brachiopod shells, Middle Devonian of China. Geochim. Cosmochim. Acta, 64, 2649–2664.

Lowenstam, H.A., 1961. Mineralogy, O^{18}/O^{16} ratios, and strontium and magnesium contents of recent and fossil brachiopods and their bearing on the history of the oceans. J. Geol., 69, 241– 260.

Mii, H.S., and Grossman, E.L., 1994. Late Pennsylvanian seasonality reflected in the ^{18}O and elemental composition of a brachiopod shell. Geology, 22, 661-664.

Mii, H.S., Grossman, E.L., and Yancey, T.E., 1999. Carboniferous isotope stratigraphies of North America: implications for Carboniferous paleoceanography and Mississippian glaciation. Geol. Soc. Am. Bull., 111, 960–973.

Mii, H-S., Grossman, E. L., Yancey, T. E., Chuvashov, B., and Egorov, A., 2001. Isotopic records of brachiopod shells from the Russian Platform – evidence for the onset of mid-Carboniferous glaciation. Chemical Geology, 175, 133-147.

Montañez, I.P., Tabor, N.J., Niemeier, D., DiMichele,W.A., Frank, T.D., Fielding, C.R., Isbell, J.L., Birgenheier, L.P., and Rygel, M.C., 2007. CO_2-forced climate and vegetation instability during Late Paleozoic deglaciation. Science, 315, 87–91.

O'Neil, J. R., Clayton, R. N., and Mayeda, T. K., 1969. Oxygen isotope fractionation in divalent metal carbonates. Journal of Chemical Physics, 51, 5547-5558.

Parkinson, D., Gordon B. Curry, G.B., Cusack, M., and Fallick, A.E., 2005. Shell structure, patterns and trends of oxygen and carbon stable isotopes in modern brachiopod shells. Chem. Geol., 219, 193– 235.

Popp, B.N., Anderson, T.F., and Sandberg, P.A., 1986. Brachiopods as indicators of original isotopic compositions in some Paleozoic limestones. Geological Society of America Bulletin, 97, 1262-1269.

Qing, H., and Veizer, J., 1994. Oxygen and carbon isotopic composition of Ordovician brachiopods: implications for coeval seawater. Geochim. Cosmochim. Acta, 58, 4429– 4442.

Railsback, L.B., 1990. Influence of changing deep ocean circulation on the Phanerozoic oxygen isotope record. Geochim. Cosmochim. Acta, 54, 1501– 1509.

Renne, P.R., Zichao, Z., Richards, M.A., Black, M.T., and Basu, A.R., 1995. Synchrony and causal relations between Permian–Triassic boundary crises and Siberian flood volcanism. Science, 269, 1413–1416.

Rush, P.F., and Chafetz, H.S., 1990. Fabric-retentive, non-luminescent brachiopods as indicators of original $\delta^{18}O$ and $\delta^{13}C$ composition: a test. J. Sediment. Petrol., 60, 968– 981.

Schidlowski, M., and Aharon, P., 1992. Carbon cycle and carbon isotope record: geochemical impact of life over 3.8 Ga of Earth history. In: Schidlowski, M., et al., (Eds.), Early Organic Evolution: Implications for Mineral and Energy Resources. Springer, Berlin, Heidelberg, pp. 147–175.

Scholle, P.A., and Arthur, M.A., 1980. Carbon isotope fluctuations in Cretaceous pelagic limestones: potential stratigraphic and petroleum exploration tool. AAPG Bull., 64, 67– 87.

Scotese, C. R. (2008). PALEOMAP Project, Climate History. http://www.scotese.com/climate.htm.

Shackleton, N. J., and Opdyke, N. D., 1973, Oxygen isotope and palaeomagnetic stratigraphy of equatorial Pacific core V28–238: Oxygen isotope temperatures and ice volumes on a 10^5 year and 10^6 year scale: Quaternary Research, 3, 39–55.

Veizer, J., Ala, D., Azmy, K., Bruckschen, P., Buhl, D., Bruhn, F., Carden, G. A. F., Diener, A., Ebneth, S., Godderis, Y., Jasper, T., Korte, C., Pawellek, F., Podlaha, O., and Strauss, H., 1999. $^{87}Sr/^{86}Sr$, $\delta^{13}C$ and $\delta^{18}O$ evolution of Phanerozoic seawater. Chemical Geology, 161, 59-88.

Veizer, J., Bruckschen, P., Pawellek, F., Diener, A., Podlaha, O.G., Carden, G.A.F., Jasper, T., Korte, C., Strauss, H., Azmy, K., and Ala, D., 1997. Oxygen isotope evolution of Phanerozoic seawater. Palaeogeography, Palaeoclimatogy, Palaeoecology, 132, 159– 172.

Veizer, J., and Mackenzie, F.T., 2004. Evolution of sedimentary rocks. In: Mackenzie, F.T. (Ed.), Sediments, Diagenesis, and Sedimentary Rocks, Treatise of Geochemistry, vol. 7, pp. 369– 407. Elsevier- Pergamon, Amsterdam.

Wallmann, K., 2001. The geological water cycle and the evolution of marine $\delta^{18}O$ values. Geochim. Cosmochim. Acta, 65, 2469– 2485.

Wallmann, K., 2004. Impact of atmospheric CO_2 and galactic cosmic radiation on Phanerozoic climate change and the marine $\delta^{18}O$ record. Geochem. Geophys. Geosyst, 5, Q06004, doi:10.1029/2003GC000683.

APPENDIX A
COMPLETE PROCEDURE DETAILS

This appendix contains the complete procedure details pertaining to this project. The procedures used were based primarily on those written by H-S. Mii (01APR94; Mii, 1996), but were adapted for use with a digital microscope camera and an image analysis system. Furthermore, certain procedures that were not specifically used in this project (i.e. partially embedding shells in Procedure B) as well as some extraneous information (e.g. general laboratory cleanup procedures) were deleted. Mii's original procedures can be obtained via *http://geoweb1.tamu.edu/faculty/grossman/DiGPaST/BrachProcedure_Mii_01APR94.pdf.* Finally, please note that I use the term "specimen" for shells and "sample" for an individual powder sample taken from a specimen.

Notes are given after certain procedures for further clarification.

Procedure A. Initial Preparation of Specimens

1. Make a list of specimens on an Excel spreadsheet, including the genus/species and all other relevant information, as well as a unique ID for each. ***NOTE: See Appendix C1.***

2. Prepare and label suitable containers for storing specimens (e.g., plastic sample box of appropriate size).

3. Photograph the specimens and labels for future reference. Include a scale (e.g., scale card or ruler).

4. Determine the best line along which the specimens should be cut for thin-sectioning and sampling, and mark it with a pen/marker/etc. This cutting plane should encompass the thickest part of the shell.

5. Determine whether the specimens will be completely or partially embedded. ***NOTE: I completely embedded all of my specimens.***

Procedure B. Embedding Specimens

NOTE: I fully embedded specimens, so I have removed the procedures for partially embedding specimens.

1. Select a suitable cardboard box for embedding specimens. Make sure that the specimens all fit in the box with at least 3 – 4 mm of space surrounding each specimen (including top and bottom). ***NOTE: I used between 3-6 specimens per box, which were on the order of 10 x 10 x 5 mm.***

2. Label the sides of the box with the specimen IDs to keep track of the specimens.

3. Mix enough epoxy to fill the box 3 - 4 mm from the bottom.

4. Place epoxy in vacuum chamber for 10 minutes at about 28-30 torr to de-gas the epoxy and prevent air pockets from forming around specimens as it cures.

5. Before putting specimens in box, pour in a 3-4 mm layer of epoxy and wait 48 hours for it to cure. This thin layer of epoxy prevents the specimens from being damaged when the bottom of the box is cut away.

6. Arrange the specimens in the box so that there is 3 - 4 mm of space around them. They should be aligned and propped up with supporting material such that the planned cutting plane of each specimen (from procedure A4) is perpendicular/parallel with the edges of the box. ***NOTE: I used yellow clay on a few specimens (which became messy) and then small pieces of Styrofoam on the rest.***

7. Mix, evacuate (see procedures B3 and B4), and pour enough epoxy to fill up the box in a layer no deeper than 2 cm and wait at least 48 hours for it to cure. Continue adding “layers” of epoxy until the specimens are completely embedded. Note that epoxy must be added in layers because it will not cure if too thick.

Procedure C. Cutting Specimens

1. After specimens are embedded and epoxy has cured, use the trim saw to separate specimens from each other and to cut away the sides of the cardboard box. Be sure to make the cuts as straight and perpendicular to each other as possible.

2. Label individual specimens with permanent marker now that they are separated.

3. Store the specimens separately in the labeled storage containers.

4. Using the Isomet saw and as thin a blade as is practical, cut the sample along the cutting line marked in procedure A4.

Procedure D. Preparing Glass Microscope Slides

NOTE: I used pre-frosted slides, so I have removed the procedures for preparing non-frosted slides.

1. Etch the sample ID on the non-frosted side of the slide(s).

2. Grind down the corners of each slide using 320-grit sandpaper and then 600-grit sandpaper. Then grind down the edges on the frosted side of each slide. This prevents you from cutting yourself while working with them and prevents the slide from "grabbing" the cloth of the polishing wheel and damaging it.

Procedure E. Making Thin-Sections

1. Determine which side of each cut specimen contains the thickest shell and proceed with that half. Store the other half in the labeled storage container.

2. Wash the specimen in distilled de-ionized water and ultrasonicate in distilled de-ionized water. Wash hands thoroughly.

3. Polish the surface of the specimen that is going to be glued to the glass slide using 320 grit polishing powder.

4. Wash the specimen in distilled de-ionized water and ultrasonicate in distilled de-ionized water. Wash hands thoroughly.

5. Polish specimen using 600 grit polishing powder.

6. Wash the specimen and glass slide in distilled de-ionized water and ultrasonicate in distilled de-ionized water. Wash hands thoroughly.

8. Glue the specimen onto the frosted side of the glass slide.

A. Using a glass stir rod spread a few drops of loctite or epoxy (no need to evacuate it) around to completely cover the surface of the specimen that will be glued. Attach specimen to slide.

B. If using loctite, put the sample(s) in the "heating box" overnight.

C. If using epoxy, allow it to cure for at least 48 hours (at room temperature).

D. Use kimwipes and absolute alcohol or acetone to wipe off the excess loctite/epoxy around the edges of the specimen after it has dried/cured.

9. Cut the specimen from the slide with the Isomet saw, leaving a thin-section roughly 500 microns thick.

10. Use the grinding wheel on the right side of the Hillquist petrographic saw to grind the thin-section to proper thickness. ***NOTE: Some of my specimens started to come off the slide during this step as a result of poor loctite/epoxy quality, so some of the thin-sections are several hundred microns thick. This problem might be avoided by heating billet in a warm oven for 24 hours and storing the billet in a desiccator for at least two hours before attaching it to the slide.***

11. Polish the thin-section(s).

A. Polish the thin-section(s) using 320 grit polishing powder.

B. Clean the thin-section(s) with the ultrasonic cleaner. Wash hands thoroughly.

D. Polish the thin-section(s) using 600 grit polishing powder.

E. Clean the thin-section(s) with the ultrasonic cleaner. Wash hands thoroughly.

F. Polish the thin-section(s) using 9.5μm polishing powder.

G. Clean the thin-section(s) with the ultrasonic cleaner. Wash hands thoroughly.

12. To see the specimen IDs better on the glass slides, mark over the specimen ID etchings with a permanent marker/pen.

Procedure F. PL/CL Photography and Specimen Preservation Analysis

NOTE: The images I acquired during these procedures can be found in Appendix B and full resolution versions can be found at http://jordan.noret.info/research/UGR.

1. Load the thin sections into the specimen compartment of the Technosyn Model 8200 MKII cathodoluminescence (CL) stage (cathodoluminoscope) and seal the compartment.

2. Turn on the cathodoluminoscope power and start the vacuum pump. Put pressure on the CL stage gun plate and door to make sure O-rings seal. Leave the vacuum pump running throughout the rest of this procedure. After the specimen chamber is sufficiently evacuated (this usually takes a minimum of 30 minutes), the electron beam will function properly.

3. While waiting for the chamber to fully evacuate, turn on the computer and digital camera attached to the microscope. Open the imaging software on the computer and center/focus the specimen on the screen using plane light in the microscope.

4. **Plane light image**. Using an exposure time that does not result in too dark or too light of an image (the brightness can be previewed on the computer monitor), capture the plane light image and save to computer. If the thin-section is of proper thickness, this exposure time should be less than 250 milliseconds (usually around 50-100 ms). Thicker sections will require longer exposures. ***NOTE: For the thicker thin-sections described in procedure E10, I had to use exposures of up to 1 second.***

5. **Cathodoluminescence image**. Turn off the microscope light, any other lights in the room, and cover the microscope with a dark cloth to prevent light from the computer monitor from leaking into the microscope stage.

   A. Turn on the electron beam (kV switch). The kV meter should read above 10 kV.

   B. Using an exposure time of 5 seconds, capture the image and save to computer.

   C. If image in previous step is too bright, try shorter exposure times. If image in previous step is too dark or completely black, try longer exposure times until a strong orange luminescence appears on the specimen (usually the calcite cements exhibit CL). Exposure times should not exceed 60 seconds.

   D. If image is still completely black, either the kV knob needs to be turned up or there is no luminescence in the specimen. Use a previously photographed luminescent specimen to determine which is the case. ***NOTE: For most thin-sections I used exposure times of***

between 10 and 20 seconds, but for the thicker thin-sections described in procedure E10, I had to use exposures of approximately 1 minute.

Step G. Powder Preparation for Stable Isotopic Analysis

1. Obtain powder samples from specimens.

   A. Select areas of shell to drill based on the PL/CL photographs, avoiding luminescent areas. Sampling locations should be distributed across whole shell. If possible, serial samples should be taken between the inner and outer shell margins.

   B. Working under a binocular microscope, use a dental drill with a stainless steel dental bur to drill holes into the shell and collect the carbonate powder residue (about 300-500 μg from each hole).

   C. Give each drill hole an ID and label a corresponding microcentrifuge tube. ***NOTE: For example, the tube corresponding to the first sample hole in specimen BT1-1 was labeled as BT1-1-1 or BT1-1(1).***

   D. Carefully sample the shell and transport the powder from each drill hole into its labeled microcentrifuge tubes.

2. Using a microbalance, take about 150 μg of each powder sample and place in a test tube to be analyzed by a stable isotope ratio mass spectrometer.

3. Follow the appropriate procedures in the stable isotope lab to analyze samples for collecting $\delta^{13}C$ and $\delta^{18}O$ data.

APPENDIX B

SPECIMEN IMAGES

This appendix contains images of each specimen used for isotopic analysis, as well as the single specimen that was characterized as luminescent, which was not analyzed. Below is a brief overview of the format followed within. Note that images were rotated, resized, and sometimes flipped in order to fit on the page neatly or for easier comparison.

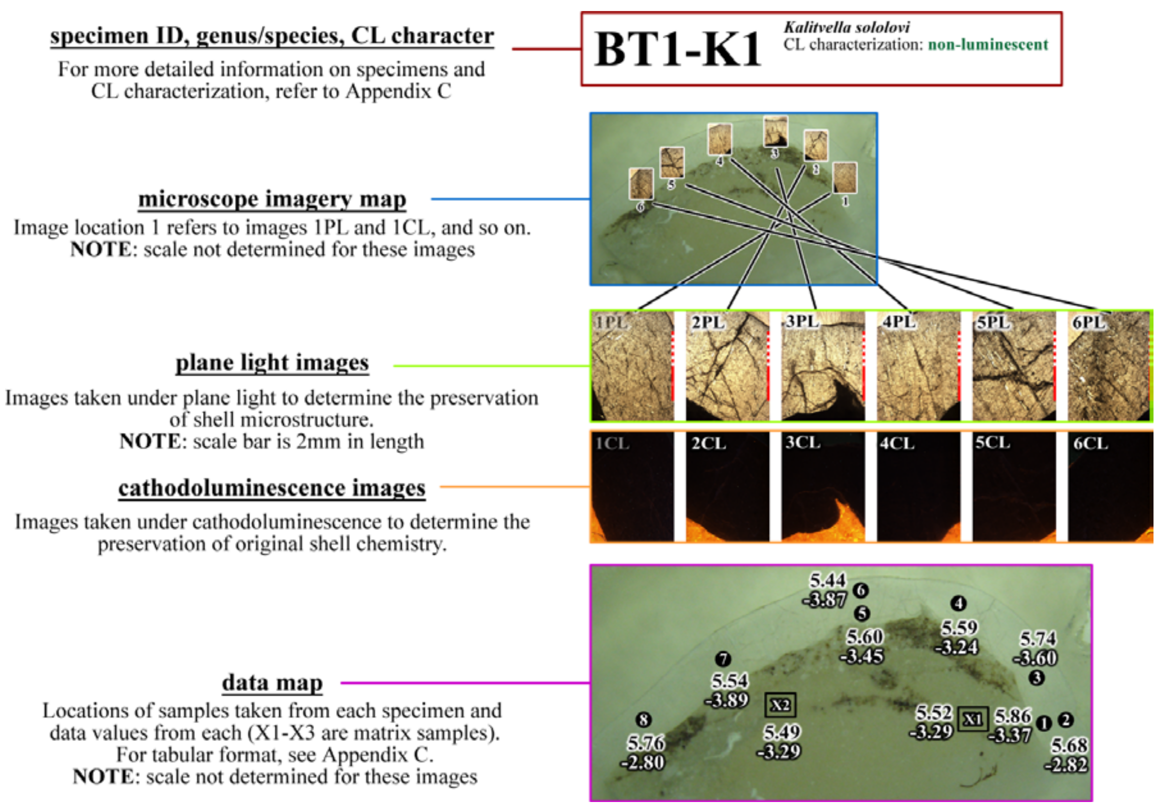

BT1-K1

Kalitvella sololovi
CL characterization: **non-luminescent**

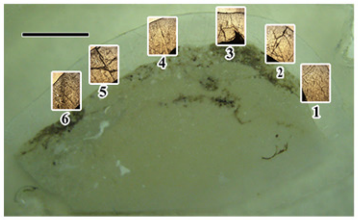

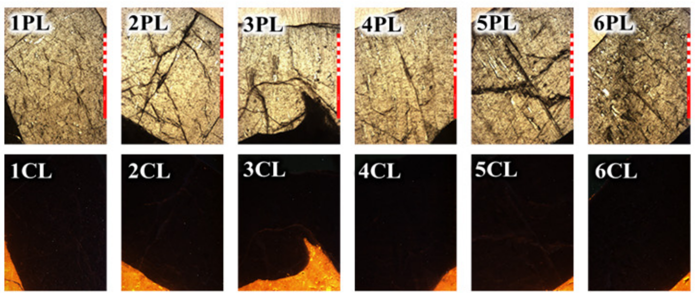

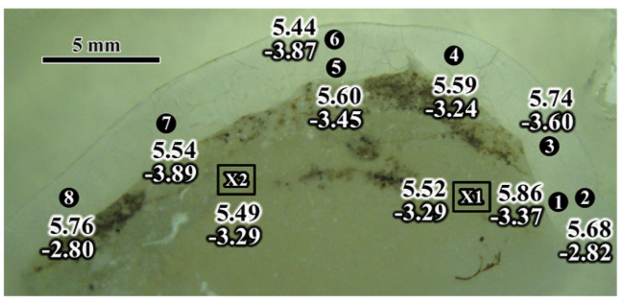

BT1-K2

Kalitvella sololovi
CL characterization: **non-luminescent**

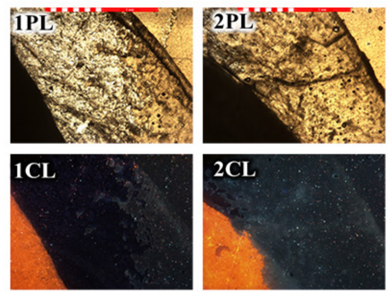

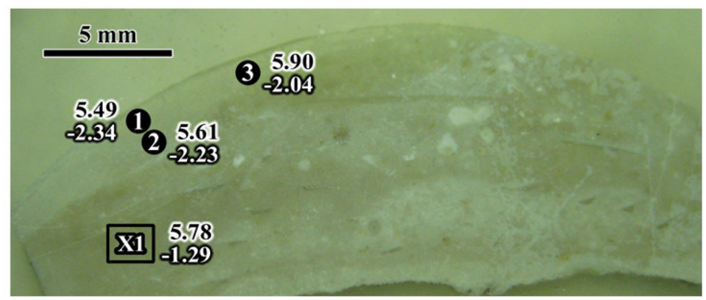

The scale bar used in PL/CL images above is 2mm in length:

Data maps: WHITE - $\delta^{18}O$ | BLACK - $\delta^{13}C$

Full resolution images can be found at: *http://jordan.noret.info/research/2009/undergrad*

BT1-1

Purdonella nikitini
CL characterization: **non-luminescent**

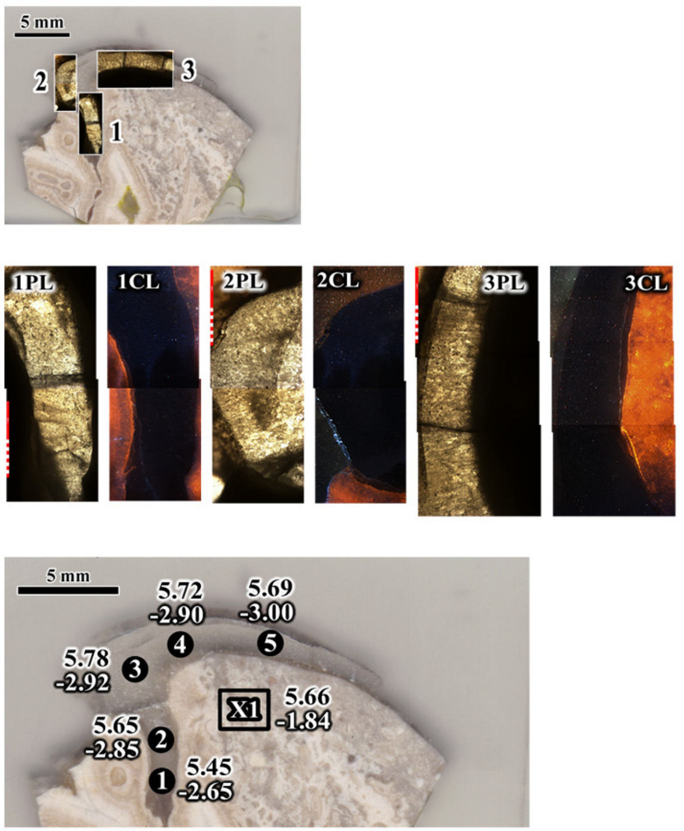

BT1-2

Purdonella nikitini
CL characterization: **non-luminescent**

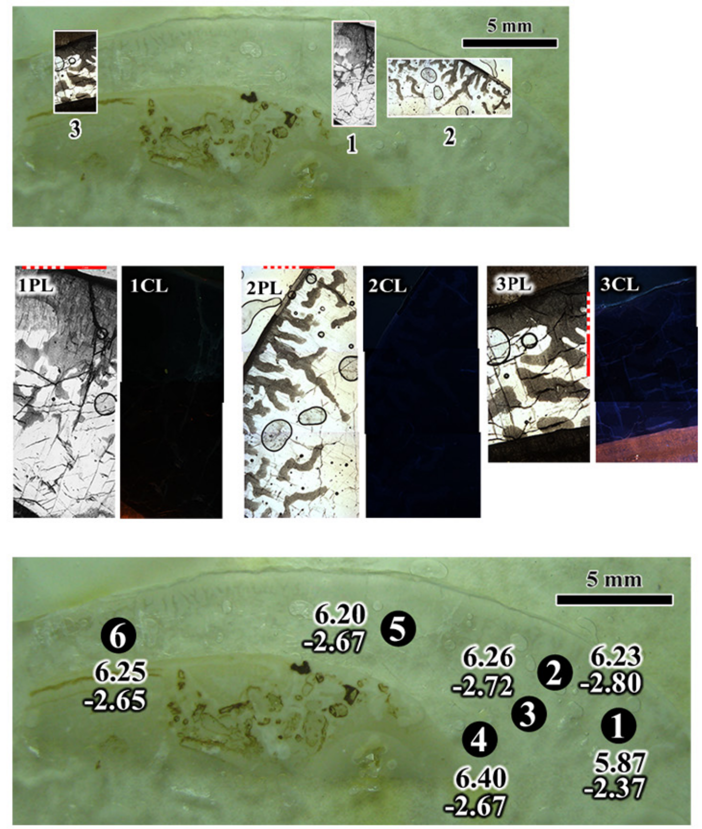

The scale bar used in PL/CL images above is 2mm in length: 1 mm

Data maps: WHITE - δ¹⁸O | BLACK - δ¹³C

Full resolution images can be found at: ***http://jordan.noret.info/research/2009/ugr***

BT1-3

Chaoiella
CL characterization: low-contrast banded luminescence

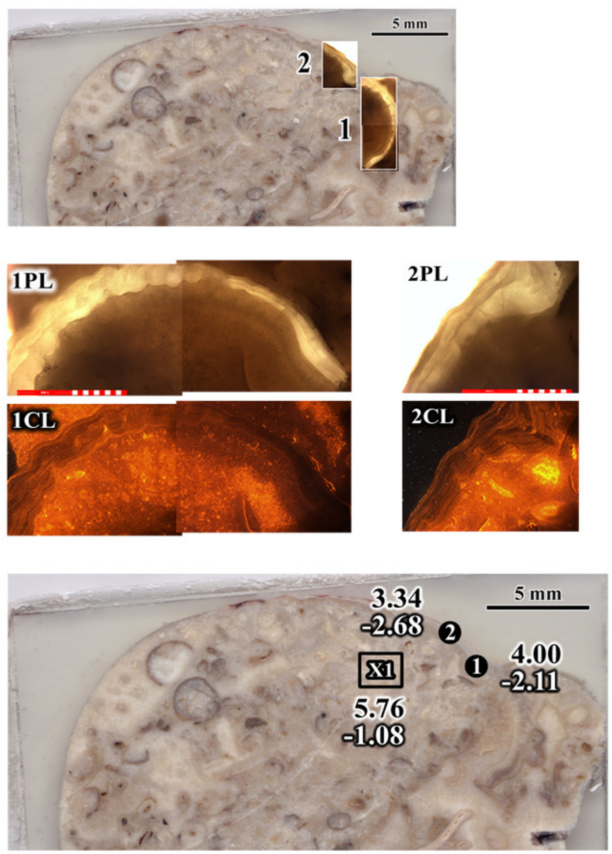

BT1-4

Chaoiella
CL characterization: low-contrast banded luminescence

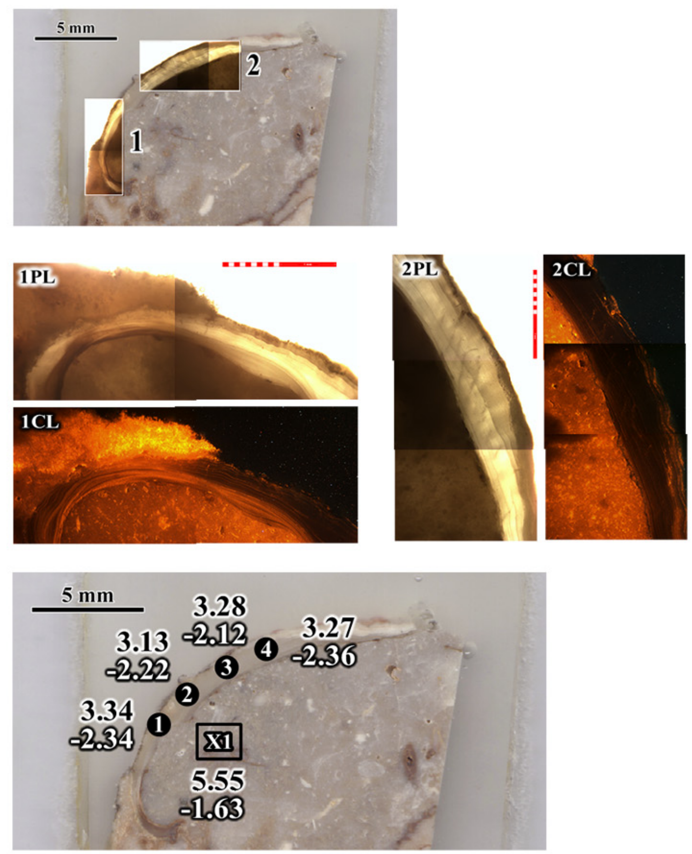

The scale bar used in PL/CL images above is 2mm in length: 1 mm

Data maps: WHITE - $\delta^{18}O$ | BLACK - $\delta^{13}C$

Full resolution images can be found at: ***http://jordan.noret.info/research/2009/ugr***

BT1-5

Stenoscisma mutabilis
CL characterization: non-luminescent

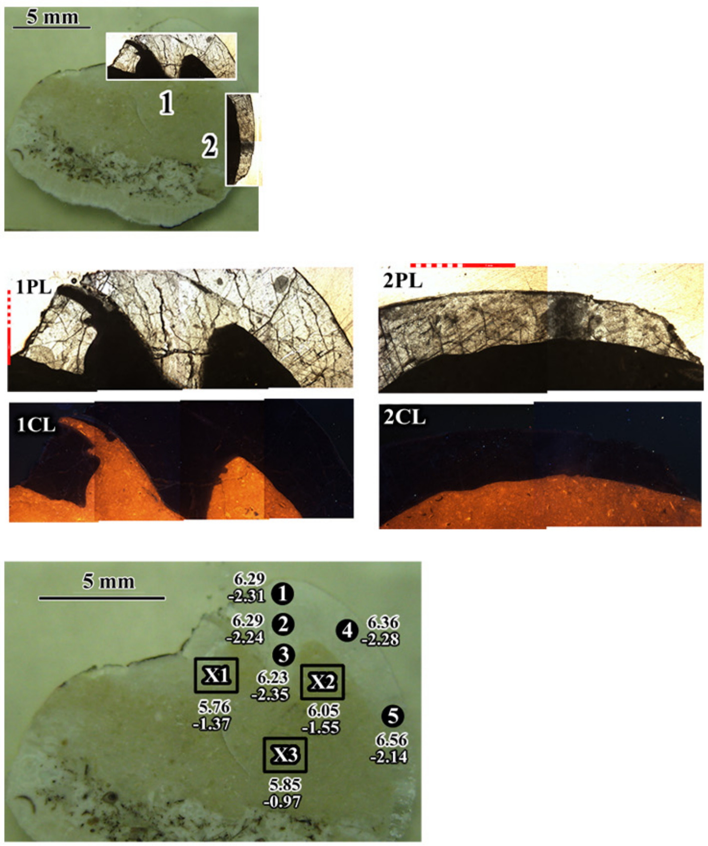

BT1-6

Stenoscisma mutabilis
CL characterization: non-luminescent

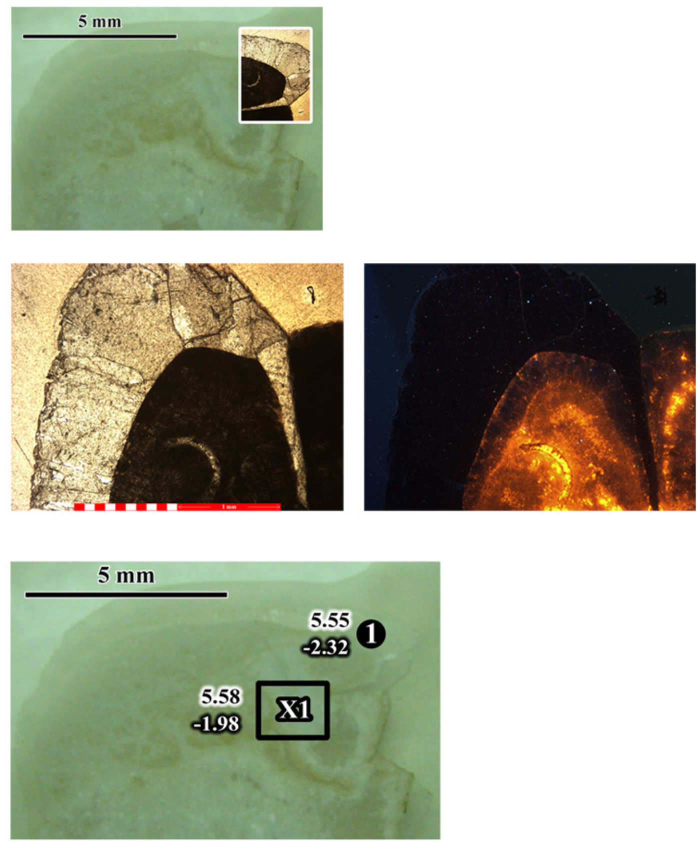

The scale bar used in PL/CL images above is 2mm in length: 1 mm

Data maps: WHITE - $\delta^{18}O$ | BLACK - $\delta^{13}C$

Full resolution images can be found at: ***http://jordan.noret.info/research/2009/ugr***

KY1

Kalitvella sololovi
CL characterization: non-luminescent

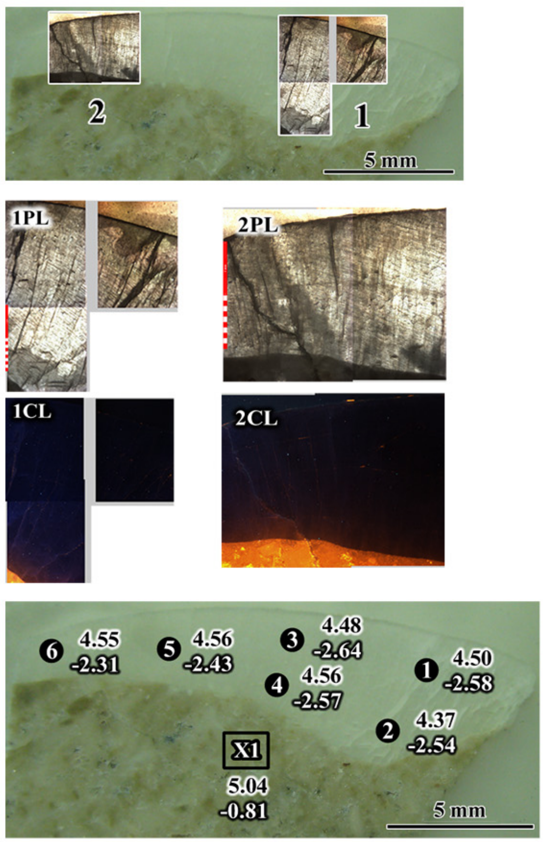

KY2

Kalitvella sololovi
CL characterization: non-luminescent

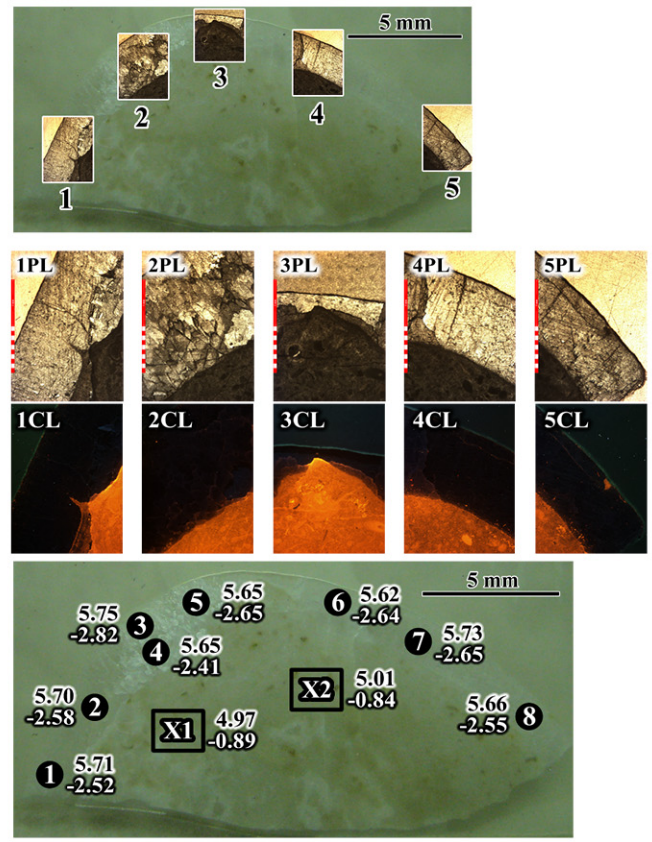

The scale bar used in PL/CL images above is 2mm in length:

Data maps: WHITE - $\delta^{18}O$ | BLACK - $\delta^{13}C$

Full resolution images can be found at: *http://jordan.noret.info/research/2009/ugr*

ST1-1

Purdonella nikitini
CL characterization: shell margin and fracture luminescence

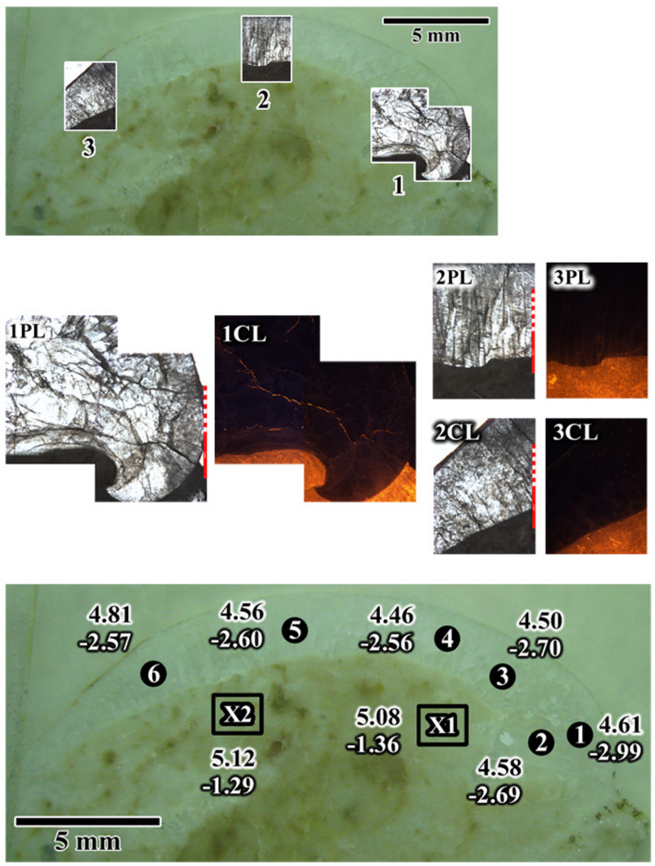

ST1-2

Purdonella nikitini
CL characterization: non-luminescent

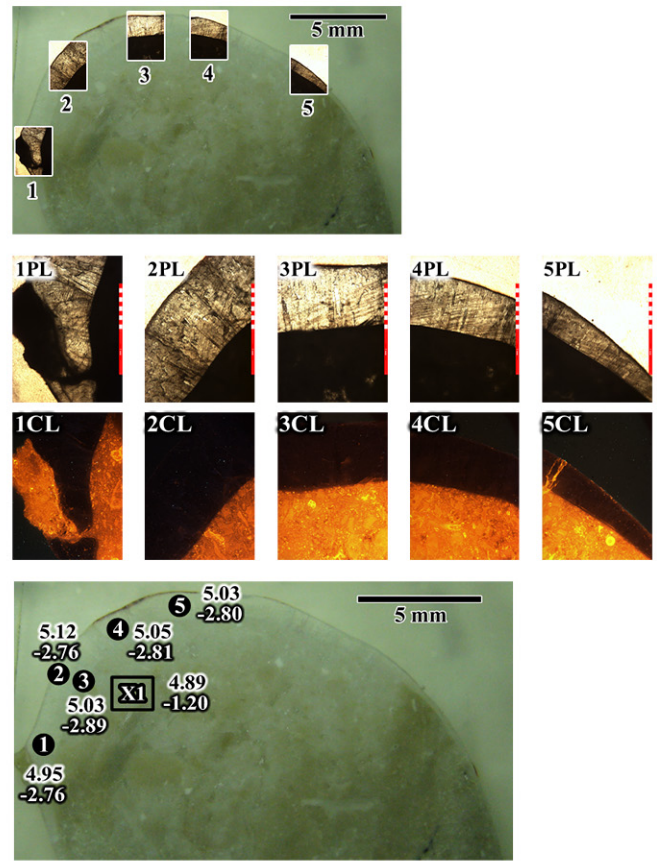

The scale bar used in PL/CL images above is 2mm in length:

Data maps: WHITE - $\delta^{18}O$ | BLACK - $\delta^{13}C$

Full resolution images can be found at: *http://jordan.noret.info/research/2009/ugr*

AA1-1

Kalitvella sp.
CL characterization: non-luminescent

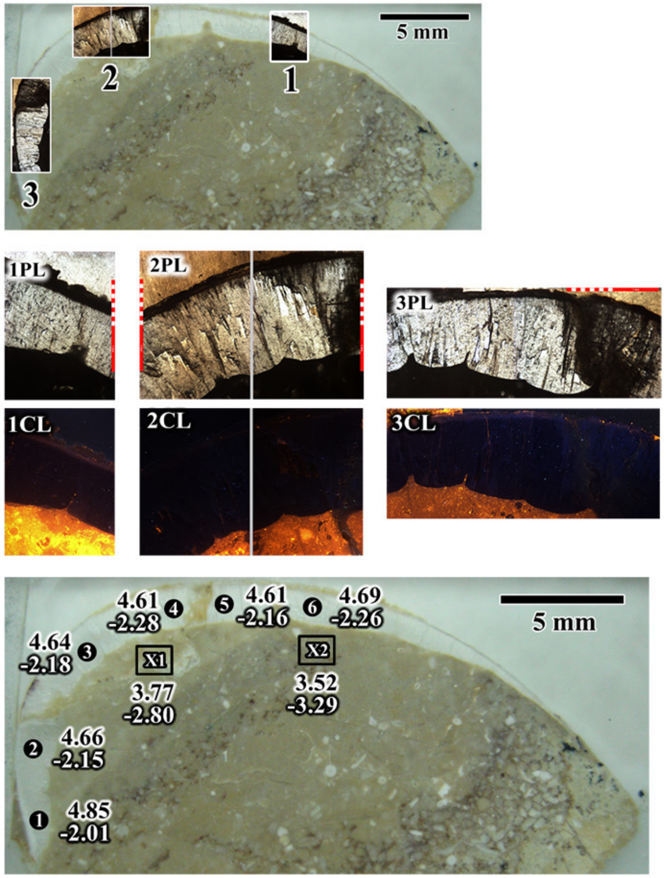

AS4-3

Stenoscisma mutabilis
CL characterization: shell margin and fracture luminescence

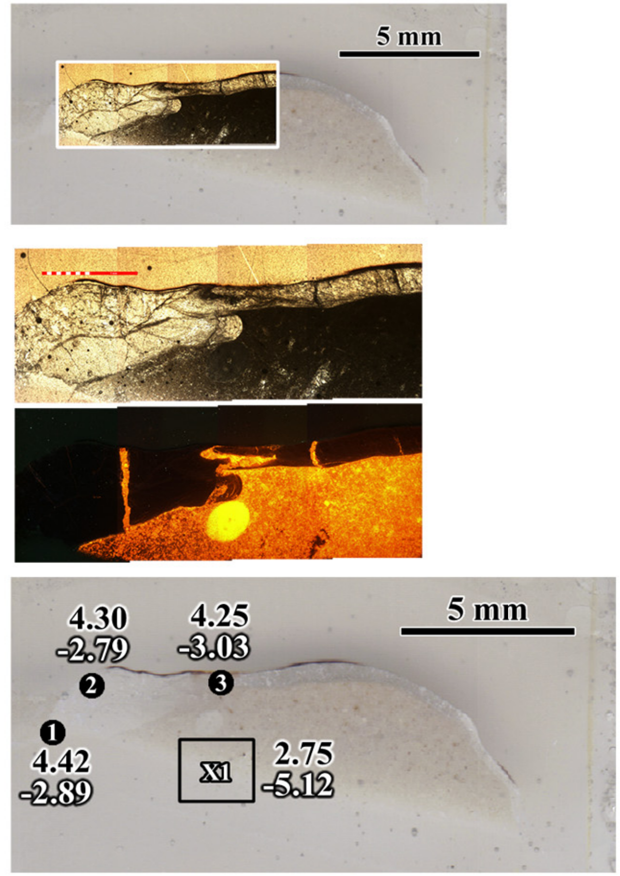

The scale bar used in PL/CL images above is 2mm in length: 1 mm

Data maps: WHITE - $\delta^{18}O$ | BLACK - $\delta^{13}C$

Full resolution images can be found at: ***http://jordan.noret.info/research/2009/ugr***

AS4-6

Chaoiella
CL characterization: low-contrast banded luminescence

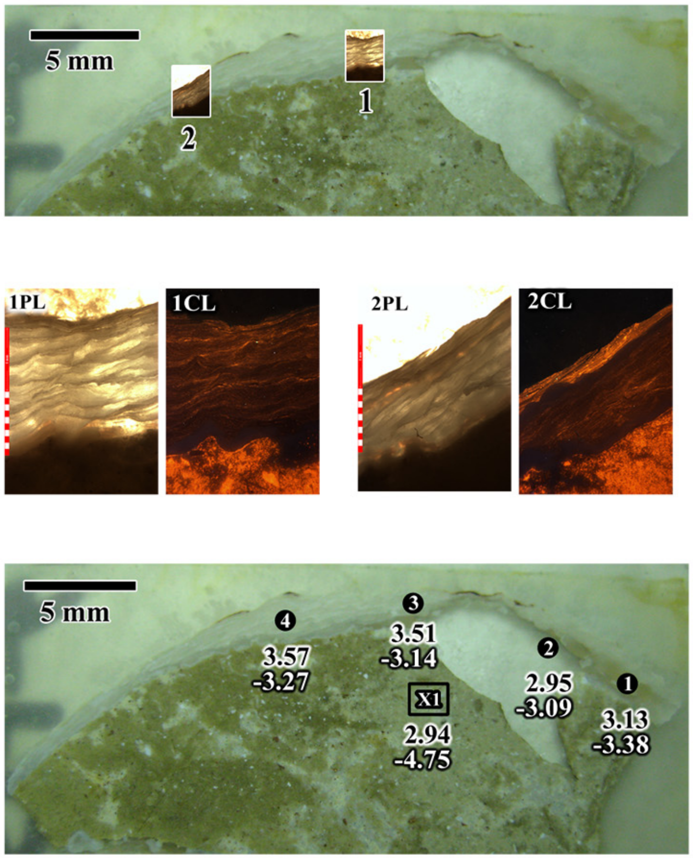

CQ13-1

Chaoiella
CL characterization: non-luminescent

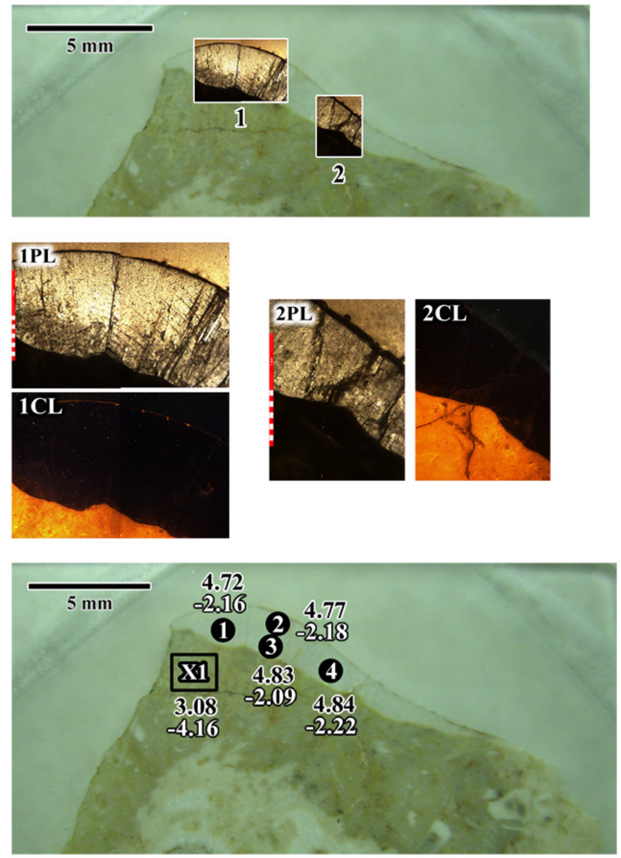

The scale bar used in PL/CL images above is 2mm in length: 1 mm

Data maps: WHITE - $\delta^{18}O$ | **BLACK -** $\delta^{13}C$

Full resolution images can be found at: ***http://jordan.noret.info/research/2009/ugr***

CQ13-2

Chaoiella
CL characterization: high-contrast banded luminescence

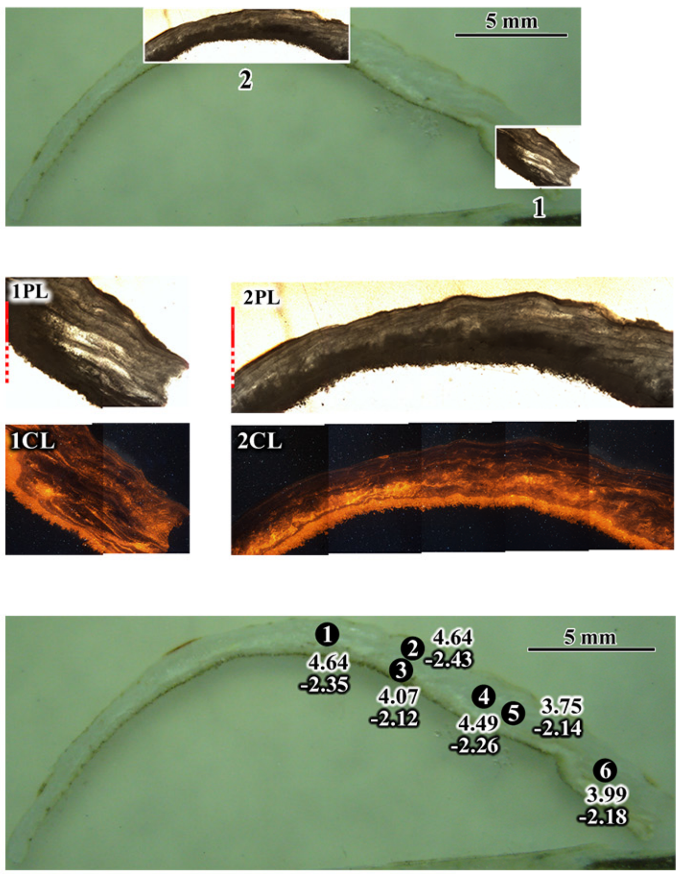

CQ12-1

Kalitvella sp.
CL characterization: shell margin and fracture luminescence

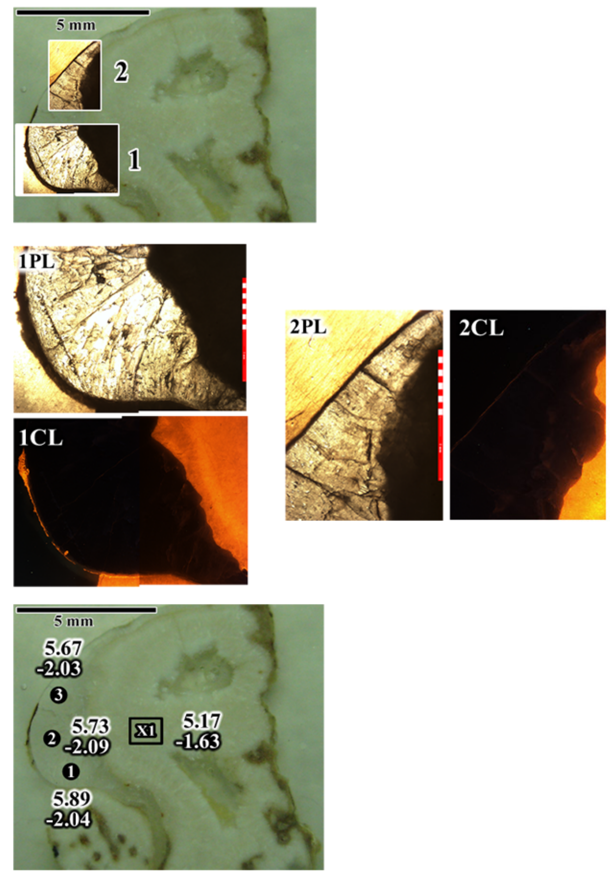

The scale bar used in PL/CL images above is 2mm in length: 1 mm

Data maps: WHITE - $\delta^{18}O$ | BLACK - $\delta^{13}C$

Full resolution images can be found at: ***http://jordan.noret.info/research/2009/ugr***

CQ12-2

Kalitvella sp.
CL characterization: shell margin and fracture luminescence

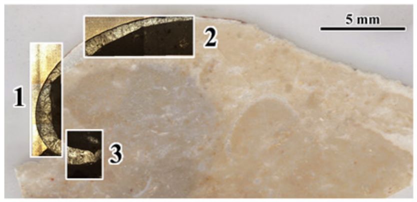

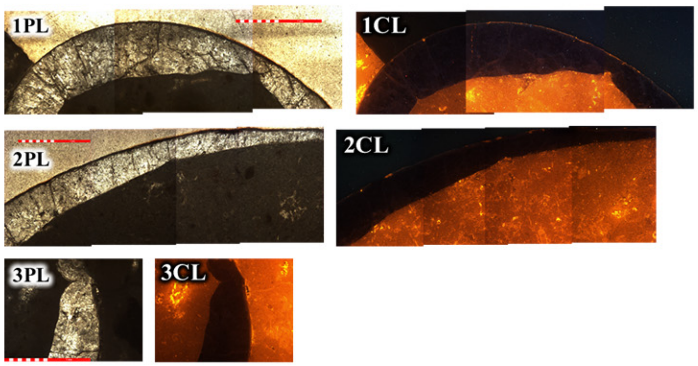

CQ15-1

Stenoscisma mutabilis
CL characterization: non-luminescent

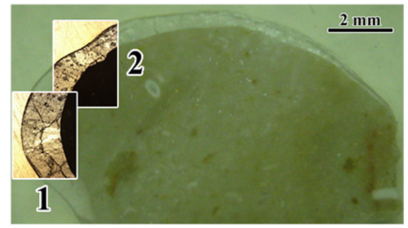

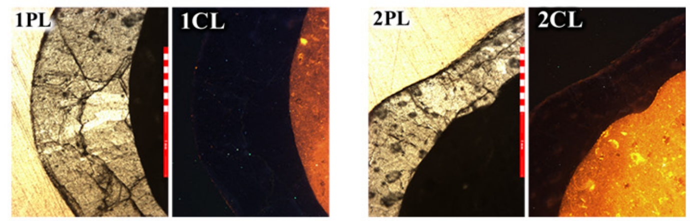

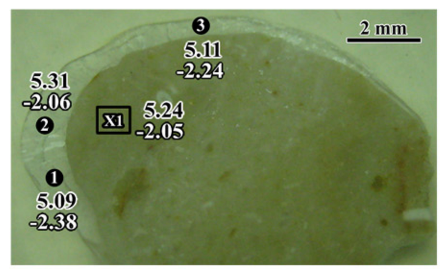

The scale bar used in PL/CL images above is 2mm in length:

Data maps: WHITE - $\delta^{18}O$ | BLACK - $\delta^{13}C$

Full resolution images can be found at: ***http://jordan.noret.info/research/2009/ugr***

CQ3-1

Chaoiella
CL characterization: luminescent
NO ISOTOPE DATA COLLECTED!

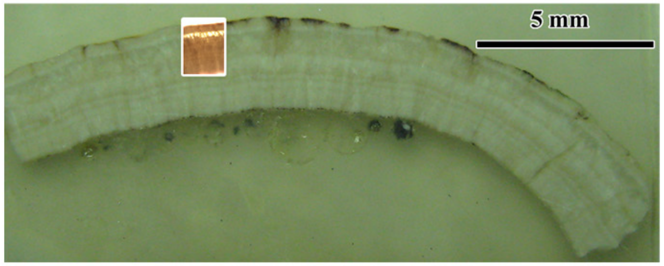

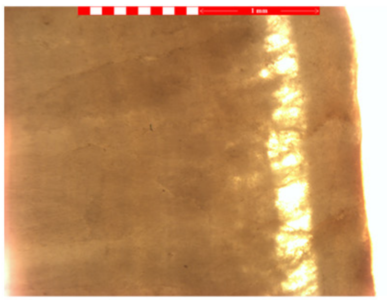

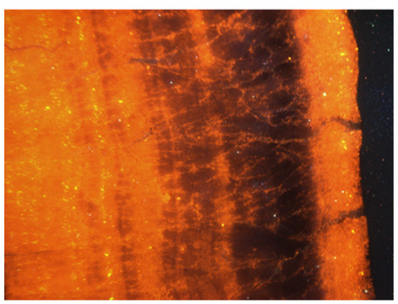

AY2-2

Chaoiella
CL characterization: high-contrast banded luminescence

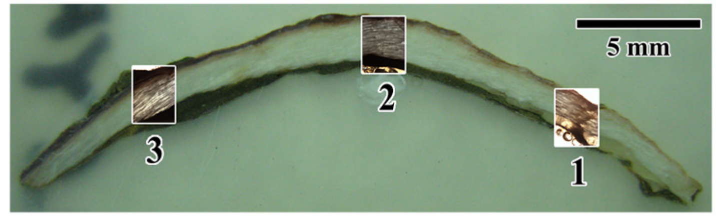

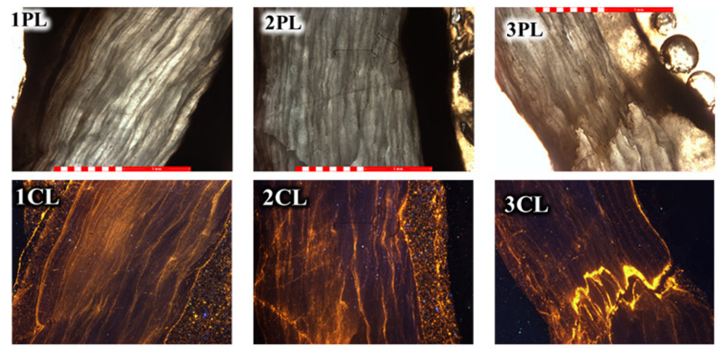

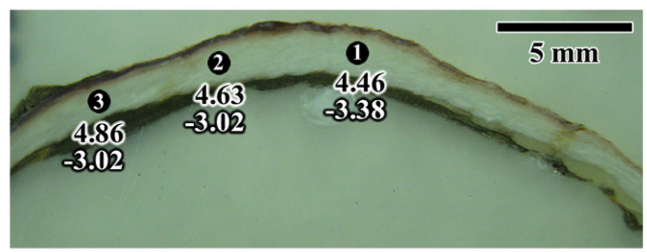

The scale bar used in PL/CL images above is 2mm in length:

Data maps: WHITE - $\delta^{18}O$ | BLACK - $\delta^{13}C$

Full resolution images can be found at: *http://jordan.noret.info/research/2009/ugr*

AY2-3

Kalitvella sp.
CL characterization: shell margin and fracture luminescence

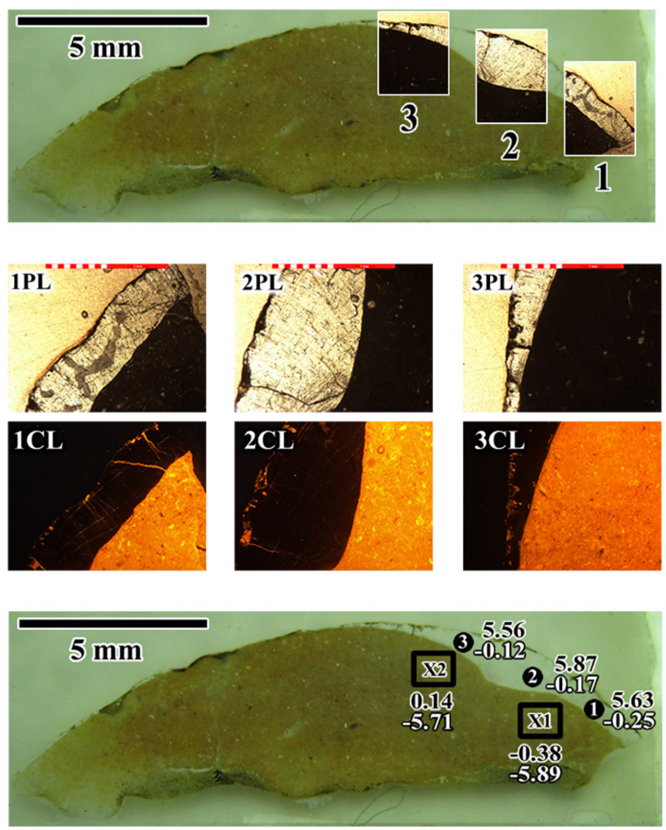

AY2-4

Kalitvella sp.
CL characterization: shell margin and fracture luminescence

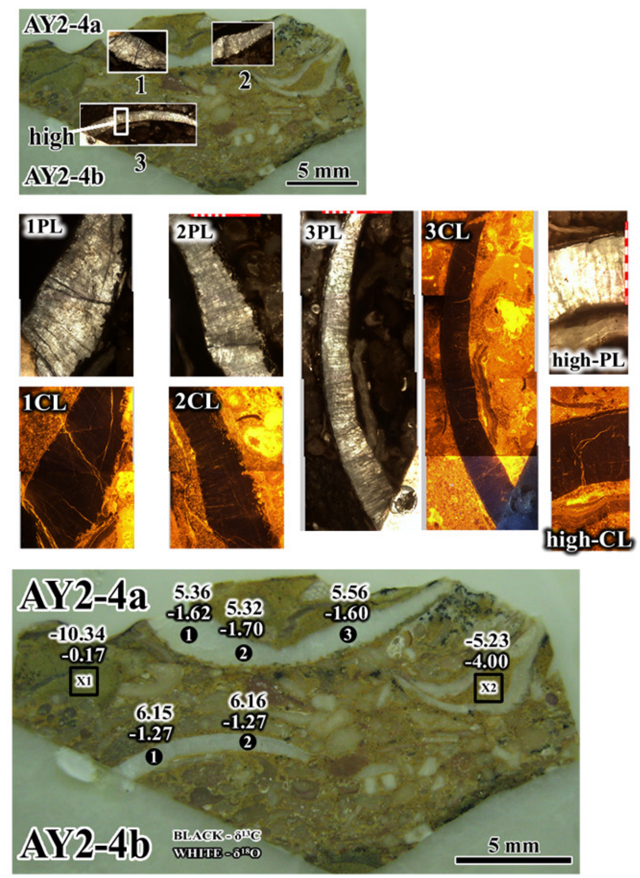

The scale bar used in PL/CL images above is 2mm in length:
The scale bar used in high-PL/CL images above is 1mm in length:

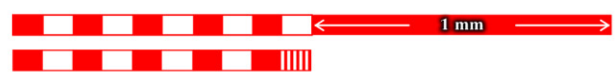

Data maps: WHITE - $\delta^{18}O$ | BLACK - $\delta^{13}C$

Full resolution images can be found at: *http://jordan.noret.info/research/2009/ugr*

AY2-6

Stenoscisma mutabilis
CL characterization: shell margin and fracture luminescence

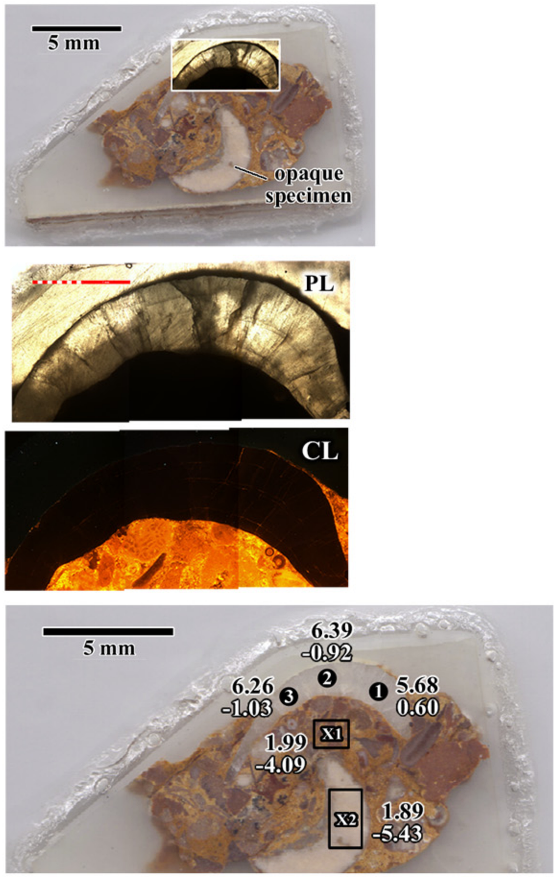

KQ1-1

Chaoiella
CL characterization: low-contrast banded luminescence

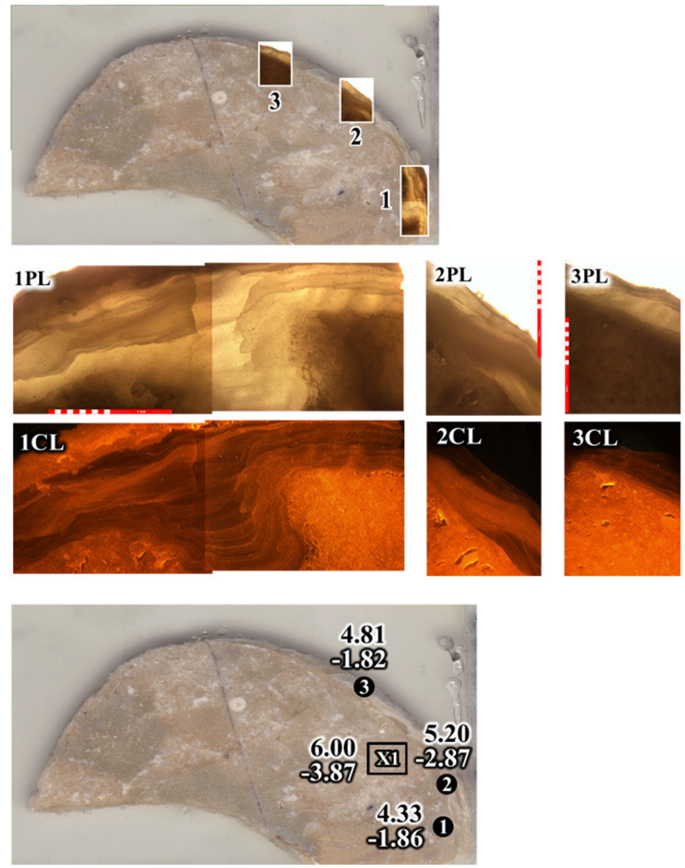

The scale bar used in PL/CL images above is 2mm in length: 1 mm

Data maps: WHITE - δ18O | **BLACK - δ13C**

Full resolution images can be found at: ***http://jordan.noret.info/research/2009/ugr***

KQ8-1

Stenoscisma mutabilis
CL characterization: shell margin and fracture luminescence

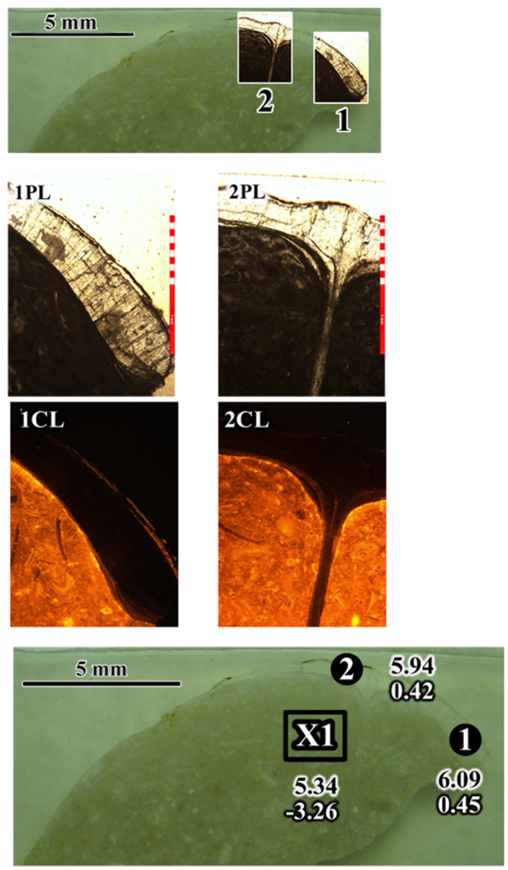

KQ8-2

Stenoscisma mutabilis
CL characterization: shell margin and fracture luminescence

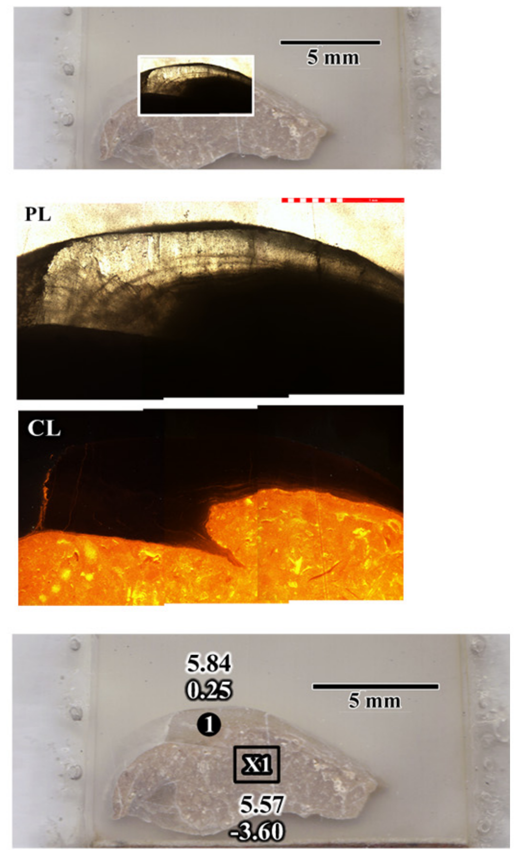

The scale bar used in PL/CL images above is 2mm in length:

Data maps: WHITE - $\delta^{18}O$ | BLACK - $\delta^{13}C$

Full resolution images can be found at: *http://jordan.noret.info/research/2009/ugr*

SQ17

Kalitvella sp.
CL characterization: shell margin and fracture luminescence

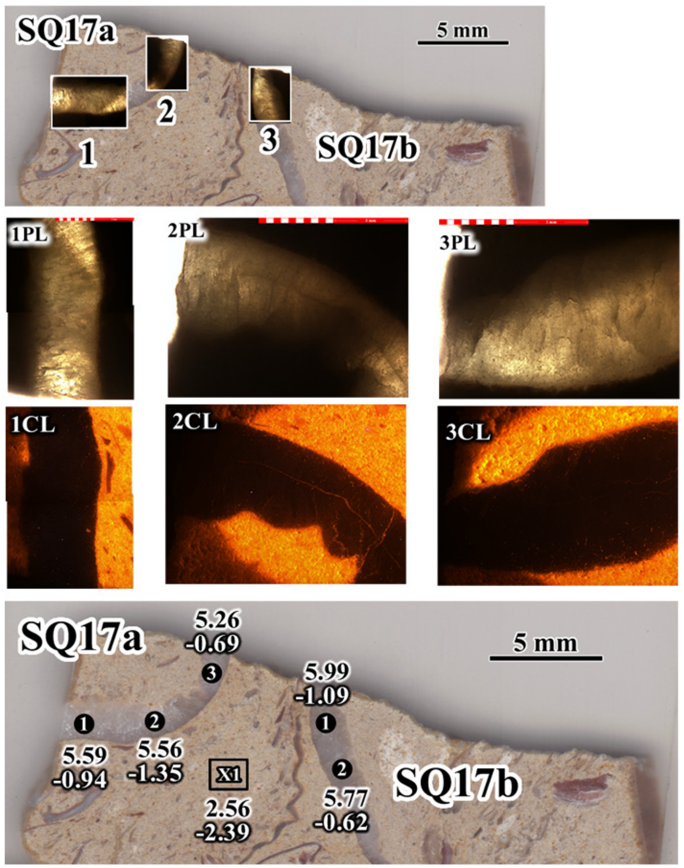

The scale bar used in PL/CL images above is 2mm in length: 

Data maps: WHITE - $\delta^{18}O$ | BLACK - $\delta^{13}C$

Full resolution images can be found at: *http://jordan.noret.info/research/2009/ugr*

APPENDIX C

SPECIMEN NOTES AND DATA

This appendix contains specific information for each specimen such as locality, stratigraphic unit, etc. All $\delta^{13}C$ and $\delta^{18}O$ data that was collected is also contained within, sorted in several different ways, as well as previously published data from Russian and North American brachiopods. All δ13C and δ18O are given in ‰ (V-PDB).

Contents:

C1) Specimen/Locality Information*

	Stage	Horizon (Formation)	Locality#	Lithology / Depositional Environment	Coordinates	Other	Taxon	Specimen ID	Age
Permian	Kungurian	Saraninian (Lower Saraninian Member)	Nizhneizginsk village, Irgina River	argillaceous micrite / interreef muds	56° 52.1'N, 57° 25.0'E		*Kalitvella sp.*	SQ17b	274.8
								SQ17a	274.8
			Chikali quarry, Sylva River, Kungur city	biomicrite / small 'reef' and bedded limestone	57° 23'N, 57° 05.9'E	17 m +	*Stensocsisma mutabilis*	KQ8-2	274.5
								KQ8-1	274.5
					57° 23'N, 57° 05.9'E	0.5 m - base of quarry	*Chaoiella*	KQ1-2	275
								KQ1-1	275
	Artinskian	Sarginskian	Mechetlino section, beside Yuresan River, near Mechetlino village	gravelly shell concentrates and poorly sorted argillaceous sands / debris flow into flysch basin (non-reef)	55° 22'N, 57° 59'E	12 m below Artinskian-Kungurian boundary, at 36 m above base of section	*Stenoscisma mutabilis*	AY2-6	275.7
								AY2-5	275.7
							Kalitvella sp.	AY2-4b	275.7
								AY2-4a	275.7
								AY2-3	275.7
							Chaoiella	AY2-2	275.7
								AY2-1	275.7
			Lebayshye quarry, Chatlik village	biomicrite & biosparite / small reef with abundant fossils	56° 48.1'N, 57° 43.7'E	*9 m above base of quarry*	*Chaoiella*	CQ3-2	276
								CQ3-1	276
						3 m above base of quarry	*Stenoscisma mutabilis*	CQ15-2	276.3
								CQ15-1	276.3
							Kalitvella sp.	CQ12-2	276.3
								CQ12-1	276.3
						5 m above base of quarry	*Chaoiella*	CQ13-2	276.5
								CQ13-1	276.5
		Irginskian	Sarana village, near spring on Ufa River, 200 m upstream from road to river from Sarana Resort	argillaceous micrite with shells / bedded limestone	56° 30.3'N, 57° 41.9'E		*Chaoiella*	AS4-6	278.6
								AS4-5	278.6
							Stenoscisma mutabilis	AS4-4	278.6
								AS4-3	278.6
							Kalitvella sp.	AS4-2	278.6
								AS4-1	278.6
		Burzevskian	Maly tau shikhan, Sterlitamak	biomicrite & biosparite / reef with abundant fossils	53° 33.9'N, 56° 04.4'E		*Kochiproductus porrectus*	AA1-4	283
								AA1-3	283
							Kalitvella sp.	AA1-2	283
								AA1-1	283
	Sakmarian	Tastubskian	Yurak tau shikhan, Sterlitamak	biomicrite & biosparite / reef with abundant fossils	53° 44.3'N, 56° 06.1'E		*Stenoscisma mutabilis*	ST1-4	293
								ST1-3	293
							Purdonella nikitini	ST1-2	293
								ST1-1	293
							Kalitvella sololovi	KY-2	293
								KY-1	293
	Asselian	Shikhanskian	Tra tau shikhan, Sterlitamak	biomicrite & biosparite / reef with abundant fossils	53° 33.2'N, 56° 05.9'E		*Stenoscisma mutabilis*	BT1-6	296
								BT1-5	296
							Chaoiella	BT1-4	296
								BT1-3	296
							Purdonella nikitini	BT1-2	296
								BT1-1	296
							Kalitvella sololovi	BT1-K2	296
								BT1-K1	296

*Samples were collected during field work done by Dr. Thomas Yancey and Dr. Boris Chuvashov. The information on this page was obtained from these individuals.
All samples are from the mid-Urals in Russia.
Ages are from Gradstein et al. 2004.

C2) Specimen Characterization and Notes

Specimen ID	Hand Sample	Microstructure	CL	Analysis Status	Notes
SQ17b	good	preserved	SMFL	analyzed	Shell shows bright luminescence along internal fractures/lineations. (These are very thin and insignificant in area, but were still avoided when drilling sample.)
SQ17a	good	preserved	SMFL	analyzed	Shell shows bright luminescence along internal fractures/lineations. (These are very thin and insignificant in area, but were still avoided when drilling sample.)
KQ8-2	good	preserved	SMFL	analyzed	Shell shows bright luminescence along internal fractures/lineations. (These areas were avoided when drilling sample.)
KQ8-1	good	preserved	SMFL	analyzed	Shell shows bright luminescence along shell margin. (These areas were avoided when drilling sample.)
KQ1-2	poor			not analyzed	Poor shell potential for isotopic analysis (shell is too thin).
KQ1-1	good	preserved	LCBL	analyzed	Shell displays low-contrast CL banding.
AY2-6	good	preserved	SMFL	analyzed	Shell shows bright luminescence along internal fractures/lineations. (These areas were avoided when drilling sample.)
AY2-5	poor			not analyzed	Poor shell potential for isotopic analysis (shell is too thin).
AY2-4b	good	preserved	SMFL	analyzed	Shell shows bright luminescence along shell margin and internal fractures/lineations. (These areas were avoided when drilling sample.)
AY2-4a	good	preserved	SMFL	analyzed	Shell shows bright luminescence along shell margin and internal fractures/lineations. (These areas were avoided when drilling sample.)
AY2-3	good	preserved	SMFL	analyzed	Shell shows bright luminescence along shell margin and internal fractures/lineations. (These areas were avoided when drilling sample.)
AY2-2	good	preserved	HCBL	analyzed	Shell displays high-contrast CL banding with lineations of brighter CL parallel to and especially along shell margins.
AY2-1	poor			not analyzed	Poor shell potential for isotopic analysis (shell is too thin).
CQ3-2	poor			not analyzed	Poor shell potential for isotopic analysis (shell is too thin).
CQ3-1	good	not preserved	L	not analyzed	Shell is opaque under plane light and nearly all of shell is luminescent under CL.
CQ15-2	poor			not analyzed	Poor shell potential for isotopic analysis (shell is too thin).
CQ15-1	good	preserved	NL	analyzed	Good shell with very minor areas of luminescence.
CQ12-2	good	preserved	SMFL	analyzed	Shell shows bright luminescence along shell margin. (These areas were avoided when drilling sample.)
CQ12-1	good	preserved	SMFL	analyzed	Shell shows bright luminescence along shell margin. (These areas were avoided when drilling sample.)
CQ13-2	good	preserved	HCBL	analyzed	Shell displays high-contrast CL banding with widespread regions of low-contrast CL banding.
CQ13-1	good	preserved	NL	analyzed	Good shell with very minor areas of luminescence.
AS4-6	good	preserved	LCBL	analyzed	Shell displays low-contrast CL banding.
AS4-5	poor			not analyzed	Poor shell potential for isotopic analysis (shell is too thin).
AS4-4	poor			not analyzed	Poor shell potential for isotopic analysis (shell is too thin).
AS4-3	good	preserved	SMFL	analyzed	Shell shows bright luminescence along several lineations perpendicular to shell margin. (These areas were avoided when drilling sample.)
AS4-2	poor			not analyzed	Poor shell potential for isotopic analysis (shell is too thin).
AS4-1	poor			not analyzed	Poor shell potential for isotopic analysis (shell is too thin).
AA1-4	poor			not analyzed	Poor shell potential for isotopic analysis (shell is too thin).
AA1-3	poor			not analyzed	Poor shell potential for isotopic analysis (shell is too thin).
AA1-2	poor			not analyzed	Poor shell potential for isotopic analysis (shell is too thin).
AA1-1	good	preserved	NL	analyzed	Good shell with very minor areas of luminescence.
ST1-4	poor			not analyzed	Poor shell potential for isotopic analysis (shell is too thin).
ST1-3	poor			not analyzed	Poor shell potential for isotopic analysis (shell is too thin).
ST1-2	good	preserved	NL	analyzed	Good shell with only one small area of luminescence (which was avoided).
ST1-1	good	preserved	SMFL	analyzed	Shell shows bright luminescence along large lineations in the beak region. (These areas were avoided when drilling sample.)
KY-2	good	preserved	NL	analyzed	Good shell with very minor areas of luminescence.
KY-1	good	preserved	NL	analyzed	Good shell with very minor areas of luminescence.
BT1-6	good	preserved	NL	analyzed	Good shell with very minor areas of luminescence.
BT1-5	good	preserved	NL	analyzed	Good shell with very minor areas of luminescence.
BT1-4	good	preserved	LCBL	analyzed	Shell displays low-contrast CL banding.
BT1-3	good	preserved	LCBL	analyzed	Shell displays low-contrast CL banding.
BT1-2	good	preserved	NL	analyzed	Good shell with very minor areas of luminescence.
BT1-1	good	preserved	NL	analyzed	Good shell with very minor areas of luminescence.
BT1-K2	good	preserved	NL	analyzed	Good shell with very minor areas of luminescence.
BT1-K1	good	preserved	NL	analyzed	Good shell with very minor areas of luminescence.

Hand samples, after cutting with an Isomet saw, were checked to determine if there was "good" potential for shell analysis (i.e. shell is thick), and were otherwise labeled "poor".

Integrity of shell microstructure is checked under plane-polarized light (See Appendix B for photographs taken).

Cathodoluminescnce (CL) is used to check the chemical preservation of the shells using the following scheme (See Appendix B for photographs taken):
L - luminescent; shell is dominantly luminescent under CL light; very little or no non-luminescent areas
LCBL - low-contrast banded luminescence ; shell displays alternating bands of strong-luminescence/weak-luminescence under CL light
HCBL - high-contrast banded luminescence; shell displays alternating bands of luminescence/non-luminescence under CL light
SMFL - shell margin and fracture luminescence ; shell mostly non-luminescent under CL light, with some luminescent areas along shell margin or fractures within shell
NL - non-luminescent; shell completely non-luminescent under CL light; no luminescent areas

C3) Summarized Specimen Data

	1. Data from all specimens						2. Data from NL and SMFL specimens						3. Data from LCBL and HCBL samples					
Specimen ID	Age	N*	$\delta^{13}C$ AVG	$\delta^{13}C$ STD	$\delta^{18}O$ AVG	$\delta^{18}O$ STD	Age	N*	$\delta^{13}C$ AVG	$\delta^{13}C$ STD	$\delta^{18}O$ AVG	$\delta^{18}O$ STD	Age	N*	$\delta^{13}C$ AVG	$\delta^{13}C$ STD	$\delta^{18}O$ AVG	$\delta^{18}O$ STD
SQ17b	274.8	2	5.88	0.16	-0.86	0.33	274.8	2	5.88	0.16	-0.86	0.33						
SQ17a	274.8	3	5.47	0.18	-0.99	0.33	274.8	3	5.47	0.18	-0.99	0.33						
KQ8-2	274.5	1	5.84		0.25		274.5	1	5.84		0.25							
KQ8-1	274.5	2	6.02	0.11	0.44	0.02	274.5	2	6.02	0.11	0.44	0.02						
KQ1-1	275	3	4.78	0.44	-2.18	0.60							275	3	4.78	0.44	-2.18	0.60
AY2-6	275.7	3	6.11	0.38	-0.45	0.91	275.7	3	6.11	0.38	-0.45	0.91						
AY2-4b	275.7	2	6.16	0.01	-1.27		275.7	2	6.16	0.01	-1.27							
AY2-4a	275.7	3	5.41	0.13	-1.64	0.05	275.7	3	5.41	0.13	-1.64	0.05						
AY2-3	275.7	3	5.93	0.33	-0.18	0.07	275.7	3	5.93	0.33	-0.18	0.07						
AY2-2	275.7	3	4.65	0.20	-3.14	0.21							275.7	3	4.65	0.20	-3.14	0.21
CQ15-1	276.3	3	5.17	0.12	-2.23	0.16	276.3	3	5.17	0.12	-2.23	0.16						
CQ12-2	276.3	4	6.01	0.13	-2.25	0.09	276.3	4	6.01	0.13	-2.25	0.09						
CQ12-1	276.3	3	5.76	0.11	-2.05	0.03	276.3	3	5.76	0.11	-2.05	0.03						
CQ13-2	276.5	6	4.26	0.38	-2.25	0.12							276.5	6	4.26	0.38	-2.25	0.12
CQ13-1	276.5	4	4.79	0.06	-2.16	0.05	276.5	4	4.79	0.06	-2.16	0.05						
AS4-6	278.6	4	3.29	0.30	-3.22	0.13							278.6	4	3.29	0.30	-3.22	0.13
AS4-3	278.6	3	4.32	0.09	-2.90	0.12	278.6	3	4.32	0.09	-2.90	0.12						
AA1-1	283	6	4.68	0.09	-2.17	0.10	283	6	4.68	0.09	-2.17	0.10						
ST1-2	293	5	5.04	0.06	-2.80	0.05	293	5	5.04	0.06	-2.80	0.05						
ST1-1	293	6	4.59	0.12	-2.69	0.16	293	6	4.59	0.12	-2.69	0.16						
KY-2	293	8	5.68	0.05	-2.60	0.12	293	8	5.68	0.05	-2.60	0.12						
KY-1	293	6	4.50	0.07	-2.51	0.12	293	6	4.50	0.07	-2.51	0.12						
BT1-6	296	1	5.55		-2.32		296	1	5.55		-2.32							
BT1-5	296	5	6.35	0.13	-2.26	0.08	296	5	6.35	0.13	-2.26	0.08						
BT1-4	296	4	3.26	0.09	-2.26	0.11							296	4	3.26	0.09	-2.26	0.11
BT1-3	296	2	3.67	0.47	-2.40	0.40							296	2	3.67	0.47	-2.40	0.40
BT1-2	296	6	6.20	0.18	-2.65	0.15	296	6	6.20	0.18	-2.65	0.15						
BT1-1	296	5	5.66	0.13	-2.86	0.13	296	5	5.66	0.13	-2.86	0.13						
BT1-K2	296	3	5.67	0.21	-2.20	0.15	296	3	5.67	0.21	-2.20	0.15						
BT1-K1	296	8	5.65	0.13	-3.38	0.42	296	8	5.65	0.13	-3.38	0.42						
AVG		30*	5.21	0.17	-2.01	0.19		24*	5.52	0.13	-1.86	0.17		6*	3.99	0.31	-2.57	0.26
STD			0.86		1.00				0.59		1.05				0.67		0.48	

4. Data from matrix

Specimen ID	Age	N*	$\delta^{13}C$ AVG	$\delta^{13}C$ STD	$\delta^{18}O$ AVG	$\delta^{18}O$ STD
SQ17	274.8	1	2.56		-2.39	
KQ8-2	274.5	1	5.57		-3.60	
KQ8-1	274.5	1	5.34		-3.26	
KQ1-1	275	1	6.00		-3.87	
AY2-6	275.7	2	1.94	0.07	-4.76	0.95
AY2-4	275.7	2	-7.79	3.61	-2.09	2.71
AY2-3	275.7	2	-0.12	0.37	-5.80	0.13
CQ15-1	276.3	1	5.24		-2.05	
CQ12-2	276.3	1	5.25		-2.35	
CQ12-1	276.3	1	5.17		-1.63	
CQ13-1	276.5	1	3.08		-4.16	
AS4-6	278.6	1	2.94		-4.75	
AS4-3	278.6	1	2.75		-5.12	
AA1-1	283	2	3.65	0.18	-3.05	0.35
ST1-2	293	1	4.89		-1.20	
ST1-1	293	2	5.10	0.03	-1.33	0.05
KY-2	293	2	4.99	0.03	-0.87	0.04
KY-1	293	1	5.04		-0.81	
BT1-6	296	1	5.58		-1.98	
BT1-5	296	3	5.89	0.15	-1.30	0.30
BT1-4	296	1	5.55		-1.63	
BT1-3	296	1	5.76		-1.08	
BT1-1	296	1	5.66		-1.84	
BT1-K2	296	1	5.78		-1.29	
BT1-K1	296	2	5.51	0.02	-3.77	0.35
AVG		25*	4.05	0.56	-2.64	0.61
STD			2.90		1.47	

Ages are from Gradstein et al. (2004).
AVG = mean
STD = 1σ

*N column displays the number of samples analyzed from each specimen However, in the bottom row the value corresponds to the total number of specimens, not the total number of analyses.

LCBL or HCBL specimen

C4) All Specimen $\delta^{13}C$ Data

	Stage	Locality	Taxon	Specimen ID	Age	δ13C (1)	δ13C (2)	δ13C (3)	δ13C (4)	δ13C (5)	δ13C (6)	δ13C (7)	δ13C (8)	N	AVG	STD	Prec-ision
Permian	Kungurian	Nizhneizginsk	*Kalitvella sp.*	SQ17b	274.8	5.99	5.77							2.00	5.88	0.16	0.06
				SQ17a	274.8	5.59	5.56	5.26						3.00	5.47	0.18	0.06
		Kungur	*Stensocsisma mutabilis*	KQ8-2	274.5	5.84								1.00	5.84	0.00	0.06
				KQ8-1	274.5	6.09	5.94							2.00	6.02	0.11	0.03
			Chaoiella	KQ1-1	275	4.33	5.20	4.81						3.00	4.78	0.44	0.06
	Artinskian	Mechetlino (paleo-shelf)	*Stenoscisma mutabilis*	AY2-6	275.7	5.68	6.39	6.26						3.00	6.11	0.38	0.06
			Kalitvella sp.	AY2-4b	275.7	6.15	6.16							2.00	6.16	0.01	0.02
				AY2-4a	275.7	5.36	5.32	5.56						3.00	5.41	0.13	0.02
				AY2-3	275.7	5.63	5.87	6.28						3.00	5.93	0.33	0.02
			Chaoiella	AY2-2	275.7	4.46	4.63	4.86						3.00	4.65	0.20	0.07
		Chatlik (paleo-reef)	*Stenoscisma mutabilis*	CQ15-1	276.3	5.09	5.31	5.11						3.00	5.17	0.12	0.06
			Kalitvella sp.	CQ12-2	276.3	6.19	5.89	5.96	5.99					4.00	6.01	0.13	0.04
				CQ12-1	276.3	5.89	5.73	5.67						3.00	5.76	0.11	0.04
			Chaoiella	CQ13-2	276.5	4.64	4.64	4.07	4.49	3.75	3.99			6.00	4.26	0.38	0.03
				CQ13-1	276.5	4.72	4.77	4.83	4.84					4.00	4.79	0.06	0.03
		Sarana	*Chaoiella*	AS4-6	278.6	3.13	2.95	3.51	3.57					4.00	3.29	0.30	0.04
			Stenoscisma mutabilis	AS4-3	278.6	4.42	4.30	4.25						3.00	4.32	0.09	0.04
		Sterlitamak	*Kalitvella sp.*	AA1-1	283	4.85	4.66	4.64	4.61	4.61	4.69			6.00	4.68	0.09	0.08
	Sakmarian	Sterlitamak	*Purdonella nikitini*	ST1-2	293	4.95	5.12	5.03	5.05	5.03				5.00	5.04	0.06	0.03
				ST1-1	293	4.61	4.58	4.50	4.46	4.56	4.81			6.00	4.59	0.12	0.08
			Kalitvella sololovi	KY-2	293	5.71	5.70	5.75	5.65	5.65	5.62	5.73	5.66	8.00	5.68	0.05	0.03
				KY-1	293	4.50	4.37	4.48	4.56	4.56	4.55			6.00	4.50	0.07	0.08
	Asselian	Sterlitamak	*Stenoscisma mutabilis*	BT1-6	296	5.55								1.00	5.55	0.00	0.02
				BT1-5	296	6.29	6.29	6.23	6.36	6.56				5.00	6.35	0.13	0.02
			Chaoiella	BT1-4	296	3.34	3.13	3.28	3.27					4.00	3.26	0.09	0.06
				BT1-3	296	4.00	3.34							2.00	3.67	0.47	0.06
			Purdonella nikitini	BT1-2	296	5.87	6.23	6.26	6.40	6.20	6.25			6.00	6.20	0.18	0.07
				BT1-1	296	5.45	5.65	5.78	5.72	5.69				5.00	5.66	0.13	0.06
			Kalitvella sololovi	BT1-K2	296	5.49	5.61	5.90						3.00	5.67	0.21	0.03
				BT1-K1	296	5.86	5.68	5.74	5.59	5.60	5.44	5.54	5.76	8.00	5.65	0.13	0.02

Each specimen was sampled as many times as was practical. δ13C (1 - 8) are the data from these different sampling locations (See Appendix B).

[shaded box] LCBL or HCBL specimen

Ages are from Gradstein et al. (2004).
N = number of different samples analyzed from each specimen.
AVG = mean
STD = 1σ
Precision = 1σ of the NBS-19 samples that were analyzed alternately with the carbonate samples of this study.

C5) All Specimen δ^{18}O Data

	Stage	Locality	Taxon	Specimen ID	Age	δ18O (1)	δ18O (2)	δ18O (3)	δ18O (4)	δ18O (5)	δ18O (6)	δ18O (7)	δ18O (8)	N	AVG	STD	Prec-ision*
Permian	Kungurian	Nizhneizginsk	*Kalitvella sp.*	SQ17b	274.8	-1.09	-0.62							2.00	-0.86	0.33	0.08
				SQ17a	274.8	-0.94	-1.35	-0.69						3.00	-0.99	0.33	0.08
		Kungur	*Stensocsisma mutabilis*	KQ8-2	274.5	0.25								1.00	0.25	0.00	0.08
				KQ8-1	274.5	0.45	0.42							2.00	0.44	0.02	0.10
			Chaoiella	KQ1-1	275	-1.86	-2.87	-1.82						3.00	-2.18	0.60	0.08
	Artinskian	Mechetlino (paleo-shelf)	*Stenoscisma mutabilis*	AY2-6	275.7	0.60	-0.92	-1.03						3.00	-0.45	0.91	0.08
			Kalitvella sp.	AY2-4b	275.7	-1.27	-1.27							2.00	-1.27	0.00	0.10
				AY2-4a	275.7	-1.62	-1.70	-1.60						3.00	-1.64	0.05	0.10
				AY2-3	275.7	-0.25	-0.17	-0.12						3.00	-0.18	0.07	0.10
			Chaoiella	AY2-2	275.7	-3.38	-3.02	-3.02						3.00	-3.14	0.21	0.11
		Chatlik (paleo-reef)	*Stenoscisma mutabilis*	CQ15-1	276.3	-2.38	-2.06	-2.24						3.00	-2.23	0.16	0.08
			Kalitvella sp.	CQ12-2	276.3	-2.13	-2.25	-2.36	-2.27					4.00	-2.25	0.09	0.06
				CQ12-1	276.3	-2.04	-2.09	-2.03						3.00	-2.05	0.03	0.06
			Chaoiella	CQ13-2	276.5	-2.35	-2.43	-2.12	-2.26	-2.14	-2.18			6.00	-2.25	0.12	0.10
				CQ13-1	276.5	-2.16	-2.18	-2.09	-2.22					4.00	-2.16	0.05	0.10
		Sarana	*Chaoiella*	AS4-6	278.6	-3.38	-3.09	-3.14	-3.27					4.00	-3.22	0.13	0.06
			Stenoscisma mutabilis	AS4-3	278.6	-2.89	-2.79	-3.03						3.00	-2.90	0.12	0.06
		Sterlitamak	*Kalitvella sp.*	AA1-1	283	-2.01	-2.15	-2.18	-2.28	-2.16	-2.26			6.00	-2.17	0.10	0.08
	Sakmarian	Sterlitamak	*Purdonella nikitini*	ST1-2	293	-2.76	-2.76	-2.89	-2.81	-2.80				5.00	-2.80	0.05	0.10
				ST1-1	293	-2.99	-2.69	-2.70	-2.56	-2.60	-2.57			6.00	-2.69	0.16	0.08
			Kalitvella sololovi	KY-2	293	-2.52	-2.58	-2.82	-2.41	-2.65	-2.64	-2.65	-2.55	8.00	-2.60	0.12	0.10
				KY-1	293	-2.58	-2.54	-2.64	-2.57	-2.43	-2.31			6.00	-2.51	0.12	0.08
	Asselian	Sterlitamak	*Stenoscisma mutabilis*	BT1-6	296	-2.32								1.00	-2.32	0.00	0.10
				BT1-5	296	-2.31	-2.24	-2.35	-2.28	-2.14				5.00	-2.26	0.08	0.10
			Chaoiella	BT1-4	296	-2.34	-2.22	-2.12	-2.36					4.00	-2.26	0.11	0.08
				BT1-3	296	-2.11	-2.68							2.00	-2.40	0.40	0.08
			Purdonella nikitini	BT1-2	296	-2.37	-2.80	-2.72	-2.67	-2.67	-2.65			6.00	-2.65	0.15	0.11
				BT1-1	296	-2.65	-2.85	-2.92	-2.90	-3.00				5.00	-2.86	0.13	0.08
			Kalitvella sololovi	BT1-K2	296	-2.34	-2.23	-2.04						3.00	-2.20	0.15	0.10
				BT1-K1	296	-3.37	-2.82	-3.60	-3.24	-3.45	-3.87	-3.89	-2.80	8.00	-3.38	0.42	0.10

Each specimen was sampled as many times as was practical. δ18O (1 - 8) are the data from these different sampling locations (See Appendix B).

[shaded] LCBL or HCBL specimen

Ages are from Gradstein et al. (2004).
N = number of different samples analyzed from each specimen.
AVG = mean
STD = 1σ
Precision = 1σ of the NBS-19 samples that were analyzed alternately with the carbonate samples of this study.

C6) All Matrix $\delta^{13}C$ and $\delta^{18}O$ Data

	Stage	Locality	Taxon	Specimen ID	Age	Prec-ision*	N	δ13C (X1)	δ13C (X2)	δ13C (X3)	δ13C AVG	δ13C STD	Prec-ision*	N	δ18O (X1)	δ18O (X2)	δ18O (X3)	δ18O AVG	δ18O STD
Permian	Kungurian	Nizhneizginsk	*Kalitvella sp.*	SQ17	274.8 / 274.8	0.06	1	2.56			2.56	0.00	0.08	1	-2.39			-2.39	0.00
		Kungur	*Stensocsisma mutabilis*	KQ8-2	274.5	0.06	1	5.57			5.57	0.00	0.08	1	-3.6			-3.60	0.00
				KQ8-1	274.5	0.03	1	5.34			5.34	0.00	0.1	1	-3.26			-3.26	0.00
			Chaoiella	KQ1-1	275	0.06	1	6			6.00	0.00	0.08	1	-3.87			-3.87	0.00
	Artinskian	Mechetlino (paleo-shelf)	*Stenoscisma mutabilis*	AY2-6	275.7	0.06	2	1.99	1.89		1.94	0.07	0.08	2	-4.09	-5.43		-4.76	0.95
			Kalitvella sp.	AY2-4	275.7 / 275.7	0.02	2	-10.34	-5.23		-7.79	3.61	0.1	2	-0.17	-4		-2.09	2.71
				AY2-3	275.7	0.02	2	-0.38	0.14		-0.12	0.37	0.1	2	-5.89	-5.71		-5.80	0.13
			Chaoiella	AY2-2	275.7									0					
		Chatlik (paleo-reef)	*Stenoscisma mutabilis*	CQ15-1	276.3	0.06	1	5.24			5.24	0.00	0.08	1	-2.05			-2.05	0.00
			Kalitvella sp.	CQ12-2	276.3	0.04	1	5.25			5.25	0.00	0.06	1	-2.35			-2.35	0.00
				CQ12-1	276.3	0.04	1	5.17			5.17	0.00	0.06	1	-1.63			-1.63	0.00
			Chaoiella	CQ13-2	276.5									0					
				CQ13-1	276.5	0.03	1	3.08			3.08	0.00	0.1	1	-4.16			-4.16	0.00
		Sarana	*Chaoiella*	AS4-6	278.6	0.04	1	2.94			2.94	0.00	0.06	1	-4.75			-4.75	0.00
			Stenoscisma mutabilis	AS4-3	278.6	0.04	1	2.75			2.75	0.00	0.06	1	-5.12			-5.12	0.00
		Sterlitamak	*Kalitvella sp.*	AA1-1	283	0.08	2	3.77	3.52		3.65	0.18	0.08	2	-2.8	-3.29		-3.05	0.35
	Sakmarian	Sterlitamak	*Purdonella nikitini*	ST1-2	293	0.03	1	4.89			4.89	0.00	0.1	1	-1.2			-1.20	0.00
				ST1-1	293	0.08	2	5.08	5.12		5.10	0.03	0.08	2	-1.36	-1.29		-1.33	0.05
			Kalitvella sololovi	KY-2	293	0.03	2	4.97	5.01		4.99	0.03	0.1	2	-0.89	-0.84		-0.87	0.04
				KY-1	293	0.08	1	5.04			5.04	0.00	0.08	1	-0.81			-0.81	0.00
	Asselian	Sterlitamak	*Stenoscisma mutabilis*	BT1-6	296	0.02	1	5.58			5.58	0.00	0.1	1	-1.98			-1.98	0.00
				BT1-5	296	0.02	3	5.76	6.05	5.85	5.89	0.15	0.1	3	-1.37	-1.55	-0.97	-1.30	0.30
			Chaoiella	BT1-4	296	0.06	1	5.55			5.55	0.00	0.08	1	-1.63			-1.63	0.00
				BT1-3	296	0.06	1	5.76			5.76	0.00	0.08	1	-1.08			-1.08	0.00
			Purdonella nikitini	BT1-2	296									0					
				BT1-1	296	0.06	1	5.66			5.66	0.00	0.08	1	-1.84			-1.84	0.00
			Kalitvella sololovi	BT1-K2	296	0.03	1	5.78			5.78	0.00	0.1	1	-1.29			-1.29	0.00
				BT1-K1	296	0.02	2	5.52	5.49		5.51	0.02	0.1	2	-3.52	-4.02		-3.77	0.35

δ13C (X1 - X3) and δ18O (X1 - X3) are samples taken from the matrix surrounding each shell analyzed.

Ages are from Gradstein et al. 2004
Precision = 1σ of the NBS-19 samples that were analyzed alternately with the carbonate samples of this study.
N = number of different analyses done on each rock.

C7) NL and SMFL Data Sorted by Stratigraphic Horizon

Specimen ID	1. Kungurian Data (Nizhneizginsk and Kungur)						2. Late Artinskian Data (Mechetlino and Chatlik)					
	Age	N*	$\delta^{13}C$ AVG	$\delta^{13}C$ STD	$\delta^{18}O$ AVG	$\delta^{18}O$ STD	Age	N*	$\delta^{13}C$ AVG	$\delta^{13}C$ STD	$\delta^{18}O$ AVG	$\delta^{18}O$ STD
SQ17b	274.8	2	5.88	0.16	-0.86	0.33						
SQ17a	274.8	3	5.47	0.18	-0.99	0.33						
KQ8-2	274.5	1	5.84		0.25							
KQ8-1	274.5	2	6.02	0.11	0.44	0.02						
KQ1-1												
AY2-6							275.7	3	6.11	0.38	-0.45	0.91
AY2-4b							275.7	2	6.16	0.01	-1.27	0.00
AY2-4a							275.7	3	5.41	0.13	-1.64	0.05
AY2-3							275.7	3	5.93	0.33	-0.18	0.07
AY2-2												
CQ15-1							276.3	3	5.17	0.12	-2.23	0.16
CQ12-2							276.3	4	6.01	0.13	-2.25	0.09
CQ12-1							276.3	3	5.76	0.11	-2.05	0.03
CQ13-2												
CQ13-1							276.5	4	4.79	0.06	-2.16	0.05
AVG	274.65	4*	5.80	0.15	-0.29	0.23	276.03	8*	5.67	0.16	-1.53	0.17
STD			0.23		0.74				0.49		0.82	

Ages are from Gradstein et al. (2004).
N = number of different samples analyzed from each specimen.
AVG = mean
STD = 1σ
Precision = 1σ of the NBS-19 samples that were analyzed alternately with the carbonate samples of this study.

*N column displays the number of samples analyzed from each specimen However, in the bottom row the value corresponds to the total number of specimens, not the total number of analyses

LCBL or HCBL specimen

7. Average Inter-Sample STD (by Horizon)

δ13C	0.40
δ18O	0.53

3. Middle Artinskian Data (Sarana)

Specimen ID	Age	N*	$\delta^{13}C$ AVG	$\delta^{13}C$ STD	$\delta^{18}O$ AVG	$\delta^{18}O$ STD
AS4-6						
AS4-3	278.6	3	4.32	0.09	-2.90	0.12
AVG	(only 1 sample)					
STD						

Specimen ID	4. Early Artinskian Data (Sterlitimak)						5. Sakmarian Data (Sterlitimak)						6. Asselian Data (Sterlitimak)					
	Age	N	$\delta^{13}C$ AVG	$\delta^{13}C$ STD	$\delta^{18}O$ AVG	$\delta^{18}O$ STD	Age	N*	$\delta^{13}C$ AVG	$\delta^{13}C$ STD	$\delta^{18}O$ AVG	$\delta^{18}O$ STD	Age	N*	$\delta^{13}C$ AVG	$\delta^{13}C$ STD	$\delta^{18}O$ AVG	$\delta^{18}O$ STD
AA1-1	283	6*	4.68	0.09	-2.17	0.10												
ST1-2							293	5	5.04	0.06	-2.80	0.05						
ST1-1							293	6	4.59	0.12	-2.69	0.16						
KY-2							293	8	5.68	0.05	-2.60	0.12						
KY-1							293	6	4.50	0.07	-2.51	0.12						
BT1-6													296	1	5.55		-2.32	
BT1-5													296	5	6.35	0.13	-2.26	0.08
BT1-4																		
BT1-3																		
BT1-2													296	6	6.20	0.18	-2.65	0.15
BT1-1													296	5	5.66	0.13	-2.86	0.13
BT1-K2													296	3	5.67	0.21	-2.20	0.15
BT1-K1													296	8	5.65	0.13	-3.38	0.42
AVG	(only 1 sample)						293.00	4*	4.95	0.08	-2.65	0.11	296.00	6*	5.85	0.16	-2.61	0.19
STD									0.54		0.12				0.34		0.45	

C8) NL and SMFL Data Sorted by Locality

Specimen ID	1. Nizhneizginsk and Kungur Data (Kungurian) Age	N*	$\delta^{13}C$ AVG	$\delta^{13}C$ STD	$\delta^{18}O$ AVG	$\delta^{18}O$ STD	2. Mechetlino Data (Late Artinskian non-reef lithology) Age	N*	$\delta^{13}C$ AVG	$\delta^{13}C$ STD	$\delta^{18}O$ AVG	$\delta^{18}O$ STD
SQ17b	274.8	2	5.88	0.16	-0.86	0.33						
SQ17a	274.8	3	5.47	0.18	-0.99	0.33						
KQ8-2	274.5	1	5.84		0.25							
KQ8-1	274.5	2	6.02	0.11	0.44	0.02						
KQ1-1												
AY2-6							275.7	3	6.11	0.38	-0.45	0.91
AY2-4b							275.7	2	6.16	0.01	-1.27	0.00
AY2-4a							275.7	3	5.41	0.13	-1.64	0.05
AY2-3							275.7	3	5.93	0.33	-0.18	0.07
AY2-2												
AVG	274.65	4*	5.80	0.15	-0.29	0.23	275.70	4*	5.90	0.21	-0.89	0.26
STD			0.23		0.74				0.34		0.68	

Specimen ID	3. Chatlik Data (Late Artinskian reef lithology) Age	N*	$\delta^{13}C$ AVG	$\delta^{13}C$ STD	$\delta^{18}O$ AVG	$\delta^{18}O$ STD	4. Sarana Data (Middle Artinskian) Age	N*	$\delta^{13}C$ AVG	$\delta^{13}C$ STD	$\delta^{18}O$ AVG	$\delta^{18}O$ STD
CQ15-1	276.3	3	5.17	0.12	-2.23	0.16						
CQ12-2	276.3	4	6.01	0.13	-2.25	0.09						
CQ12-1	276.3	3	5.76	0.11	-2.05	0.03						
CQ13-2												
CQ13-1	276.5	4	4.79	0.06	-2.16	0.05						
AS4-6												
AS4-3							278.6	3	4.32	0.09	-2.90	0.12
AVG	276.35	4*	5.43	0.11	-2.17	0.09	(only 1 sample)					
STD			0.55		0.09							

Specimen ID	5. Sterlitamak Data (Early Artinskian) Age	N	$\delta^{13}C$ AVG	$\delta^{13}C$ STD	$\delta^{18}O$ AVG	$\delta^{18}O$ STD	6. Sterlitamak Data (Sakmarian) Age	N*	$\delta^{13}C$ AVG	$\delta^{13}C$ STD	$\delta^{18}O$ AVG	$\delta^{18}O$ STD	7. Sterlitamak Data (Asselian) Age	N*	$\delta^{13}C$ AVG	$\delta^{13}C$ STD	$\delta^{18}O$ AVG	$\delta^{18}O$ STD
AA1-1	283	6*	4.68	0.09	-2.17	0.10												
ST1-2							293	5	5.04	0.06	-2.80	0.05						
ST1-1							293	6	4.59	0.12	-2.69	0.16						
KY-2							293	8	5.68	0.05	-2.60	0.12						
KY-1							293	6	4.50	0.07	-2.51	0.12						
BT1-6													296	1	5.55		-2.32	
BT1-5													296	5	6.35	0.13	-2.26	0.08
BT1-4																		
BT1-3																		
BT1-2													296	6	6.20	0.18	-2.65	0.15
BT1-1													296	5	5.66	0.13	-2.86	0.13
BT1-K2													296	3	5.67	0.21	-2.20	0.15
BT1-K1													296	8	5.65	0.13	-3.38	0.42
AVG	(only 1 sample)						293.00	4*	4.95	0.08	-2.65	0.11	296.00	6*	5.85	0.16	-2.61	0.19
STD									0.54		0.12				0.34		0.45	

Ages are from Gradstein et al. (2004).
N = number of different samples analyzed from each specimen.
AVG = mean
STD = 1σ
Precision = 1σ of the NBS-19 samples that were analyzed alternately with the carbonate samples of this study.

*N column displays the number of samples analyzed from each specimen However, in the bottom row the value corresponds to the total number of specimens, not the total number of

(shaded) LCBL or HCBL specimen

C9) Matrix Data Sorted by Stratigraphic Horizon

Specimen ID	1. Kungurian Data (Nizhneizginsk and Kungur)						2. Late Artinskian Data (Mechetlino and Chatlik)					
	Age	N*	δ^{13}C AVG	δ^{13}C STD	δ^{18}O AVG	δ^{18}O STD	Age	N*	δ^{13}C AVG	δ^{13}C STD	δ^{18}O AVG	δ^{18}O STD
SQ17	274.8	1	2.56		-2.39							
KQ8-2	274.5	1	5.57		-3.60							
KQ8-1	274.5	1	5.34		-3.26							
KQ1-1	275	1	6.00		-3.87							
AY2-6							275.7	2	1.94	0.07	-4.09	-5.43
AY2-4							275.7	#	#	#	#	#
AY2-3							275.7	2	-0.12	0.37	-5.80	0.13
CQ15-1							276.3	1	5.24		-2.05	
CQ12-2							276.3	1	5.25		-2.35	
CQ12-1							276.3	1	5.17		-1.63	
CQ13-1							276.5	1	3.08		-4.16	
AVG	274.70	4*	4.87		-3.28		276.07	6	3.43	0.22	-3.35	-2.65
STD			1.56		0.64				2.22		1.60	

Ages are from Gradstein et al. (2004).
AVG = mean
STD = 1σ

*N column displays the number of analyses done on each sample. However, in the bottom row the value corresponds to the total number of samples (# Samples), not the total number of analyses.

#Data was removed because the values were extremely anomalous (see Appendix C6).

3. Middle Artinskian Data (Sarana)

Specimen ID	Age	N*	δ^{13}C AVG	δ^{13}C STD	δ^{18}O AVG	δ^{18}O STD
AS4-6	278.6	1	2.94		-4.75	
AS4-3	278.6	1	2.75		-5.12	
AVG	278.60	2*	2.85		-4.94	
STD			0.13		0.26	

Specimen ID	4. Early Artinskian Data (Sterlitimak)						5. Sakmarian Data (Sterlitimak)						6. Asselian Data (Sterlitimak)					
	Age	N	δ^{13}C AVG	δ^{13}C STD	δ^{18}O AVG	δ^{18}O STD	Age	N*	δ^{13}C AVG	δ^{13}C STD	δ^{18}O AVG	δ^{18}O STD	Age	N*	δ^{13}C AVG	δ^{13}C STD	δ^{18}O AVG	δ^{18}O STD
AA1-1	283	2*	3.65	0.18	-3.05	0.35												
ST1-2							293	1	4.89		-1.20							
ST1-1							293	2	5.10	0.03	-1.33	0.05						
KY-2							293	2	4.99	0.03	-0.87	0.04						
KY-1							293	1	5.04		-0.81							
BT1-6													296	1	5.58		-1.98	
BT1-5													296	3	5.89	0.15	-1.30	0.30
BT1-4													296	1	5.55		-1.63	
BT1-3													296	1	5.76		-1.08	
BT1-1													296	1	5.66		-1.84	
BT1-K2													296	1	5.78		-1.29	
BT1-K1													296	2	5.51	0.02	-3.77	0.35
AVG	(only 1 sample)						293.00	4*	5.01	0.03	-1.05	0.04	296.00	7*	5.67	0.08	-1.84	0.33
STD									0.09		0.25				0.14		0.91	

C10) Matrix Data Sorted by Locality

Ages are from Gradstein et al. (2004).
AVG = mean
STD = 1σ

*N column displays the number of analyses done on each sample. However, in the bottom row the value corresponds to the total number of samples (# Samples), not the total number of analyses.

#Data was removed because the values were extremely anomalous (see Appendix C6).

	1. Nizhneizginsk and Kungur Data (Kungurian)						2. Mechetlino Data (Late Artinskian non-reef lithology)					
Specimen ID	Age	N*	$\delta^{13}C$ AVG	$\delta^{13}C$ STD	$\delta^{18}O$ AVG	$\delta^{18}O$ STD	Age	N*	$\delta^{13}C$ AVG	$\delta^{13}C$ STD	$\delta^{18}O$ AVG	$\delta^{18}O$ STD
SQ17	274.8	1	2.56		-2.39							
KQ8-2	274.5	1	5.57		-3.60							
KQ8-1	274.5	1	5.34		-3.26							
KQ1-1	275	1	6.00		-3.87							
AY2-6							275.7	2	1.94	0.07	-4.09	-5.43
AY2-4							275.7	#	#	#	#	#
AY2-3							275.7	2	-0.12	0.37	-5.80	0.13
AVG	274.70	4*	4.87		-3.28		275.70	3*	0.91	0.22	-4.95	-2.65
STD			1.56		0.64				1.46		1.21	

	3. Chatlik Data (Late Artinskian reef lithology)						4. Sarana Data (Middle Artinskian)					
Specimen ID	Age	N*	$\delta^{13}C$ AVG	$\delta^{13}C$ STD	$\delta^{18}O$ AVG	$\delta^{18}O$ STD	Age	N*	$\delta^{13}C$ AVG	$\delta^{13}C$ STD	$\delta^{18}O$ AVG	$\delta^{18}O$ STD
CQ15-1	276.3	1	5.24		-2.05							
CQ12-2	276.3	1	5.25		-2.35							
CQ12-1	276.3	1	5.17		-1.63							
CQ13-1	276.5	1	3.08		-4.16							
AS4-6							278.6	1	2.94		-4.75	
AS4-3							278.6	1	2.75		-5.12	
AVG	276.35	4*	4.69		-2.55		278.60	2*	2.85		-4.94	
STD			1.07		1.11				0.13		0.26	

	5. Sterlitamak Data (Early Artinskian)						6. Sterlitamak Data (Sakmarian)						7. Sterlitamak Data (Asselian)					
Specimen ID	Age	N	$\delta^{13}C$ AVG	$\delta^{13}C$ STD	$\delta^{18}O$ AVG	$\delta^{18}O$ STD	Age	N*	$\delta^{13}C$ AVG	$\delta^{13}C$ STD	$\delta^{18}O$ AVG	$\delta^{18}O$ STD	Age	N*	$\delta^{13}C$ AVG	$\delta^{13}C$ STD	$\delta^{18}O$ AVG	$\delta^{18}O$ STD
AA1-1	283	2*	3.65	0.18	-3.05	0.35												
ST1-2							293	1	4.89		-1.20							
ST1-1							293	2	5.10	0.03	-1.33	0.05						
KY-2							293	2	4.99	0.03	-0.87	0.04						
KY-1							293	1	5.04		-0.81							
BT1-6													296	1	5.58		-1.98	
BT1-5													296	3	5.89	0.15	-1.30	0.30
BT1-4													296	1	5.55		-1.63	
BT1-3													296	1	5.76		-1.08	
BT1-1													296	1	5.66		-1.84	
BT1-K2													296	1	5.78		-1.29	
BT1-K1													296	2	5.51	0.02	-3.77	0.35
AVG	(only 1 sample)						293.00	4*	5.01	0.03	-1.05	0.04	296.00	7*	5.67	0.08	-1.84	0.33
STD									0.09		0.25				0.14		0.91	

C11) Data Sorted by Specimen Genus

Specimen ID	1. *Kalitvella* Data: Age	N	$\delta^{13}C$ AVG	$\delta^{13}C$ STD	$\delta^{18}O$ AVG	$\delta^{18}O$ STD	2. *Stenoscisma* Data: Age	N	$\delta^{13}C$ AVG	$\delta^{13}C$ STD	$\delta^{18}O$ AVG	$\delta^{18}O$ STD	3. *Chaoiella* Data: Age	N	$\delta^{13}C$ AVG	$\delta^{13}C$ STD	$\delta^{18}O$ AVG	$\delta^{18}O$ STD
SQ17b	274.8	2	5.88	0.16	-0.86	0.33												
SQ17a	274.8	3	5.47	0.18	-0.99	0.33												
KQ8-2							274.5	1	5.84		0.25	0.00						
KQ8-1							274.5	2	6.02	0.11	0.44	0.02						
KQ1-1													275	3	4.78	0.44	-2.18	0.60
AY2-6							275.7	3	6.11	0.38	-0.45	0.91						
AY2-4b	275.7	2	6.16	0.01	-1.27	0.00												
AY2-4a	275.7	3	5.41	0.13	-1.64	0.05												
AY2-3	275.7	3	5.93	0.33	-0.18	0.07												
AY2-2													275.7	3	4.65	0.20	-3.14	0.21
CQ15-1							276.3	3	5.17	0.12	-2.23	0.16						
CQ12-2	276.3	4	6.01	0.13	-2.25	0.09												
CQ12-1	276.3	3	5.76	0.11	-2.05	0.03												
CQ13-2													276.5	6	4.26	0.38	-2.25	0.12
CQ13-1													276.5	4	4.79	0.06	-2.16	0.05
AS4-6													278.6	4	3.29	0.30	-3.22	0.13
AS4-3							278.6	3	4.32	0.09	-2.90	0.12						
AA1-1	283	6	4.68	0.09	-2.17	0.10												
KY-2	293	8	5.68	0.05	-2.60	0.12												
KY-1	293	6	4.50	0.07	-2.51	0.12												
BT1-6							296	1	5.55		-2.32							
BT1-5							296	5	6.35	0.13	-2.26	0.08						
BT1-4													296	4	3.26	0.09	-2.26	0.11
BT1-3													296	2	3.67	0.47	-2.40	0.40
BT1-K2	296	3	5.67	0.21	-2.20	0.15												
BT1-K1	296	8	5.65	0.13	-3.38	0.42												
AVG	282.53		5.57	0.13	-1.84	0.15	281.66		5.62	0.16	-1.35	0.22	282.04		4.10	0.27	-2.52	0.23
STD			0.50		0.89				0.69		1.39				0.69		0.46	

4. *Purdonella* Data

Specimen ID	Age	N	$\delta^{13}C$ AVG	$\delta^{13}C$ STD	$\delta^{18}O$ AVG	$\delta^{18}O$ STD
ST1-2	293	5	5.04	0.06	-2.80	0.05
ST1-1	293	6	4.59	0.12	-2.69	0.16
BT1-2	296	6	6.20	0.18	-2.65	0.15
BT1-1	296	5	5.66	0.13	-2.86	0.13
AVG	294.50		5.37	0.12	-2.75	0.12
STD			0.71		0.10	

Ages are from Gradstein et al. (2004).
N = number of different samples analyzed from each specimen.
AVG = mean
STD = 1σ

*N column displays the number of samples analyzed from each specimen However, in the bottom row the value corresponds to the total number of specimens, not the total number of

(shaded) LCBL or HCBL specimen

C12) Previously Published Data

1. Previously published Uralian brachiopod data

Specimen	Location	Age (STD 02)	$\delta^{13}C$	$\delta^{18}O$	Reference
ru 7	Usolka	295.62	4.94	-2.26	Korte et al. (2005)
ru 9	Usolka	294.36	4.52	-0.22	Korte et al. (2005)
ru 9	Usolka	294.36	3.56	-0.37	Korte et al. (2005)
ru 25	Usolka	294.06	4.60	-0.16	Korte et al. (2005)
ru 8	Usolka	293.77	4.72	-0.26	Korte et al. (2005)
ru 28	Usolka	293.07	4.34	0.08	Korte et al. (2005)
ru 29	Usolka	291.61	3.89	-0.10	Korte et al. (2005)
ru 10	Usolka	291.48	4.55	-0.94	Korte et al. (2005)
ru 11	Usolka	289.65	3.25	-1.06	Korte et al. (2005)
ru 12	Usolka	288.85	5.39	-1.62	Korte et al. (2005)
ru 13	Usolka	287.56	4.16	-2.85	Korte et al. (2005)
ru 13	Usolka	287.56	4.38	-2.57	Korte et al. (2005)
ru 20	Sakmara	285.50	4.30	-2.22	Korte et al. (2005)
ru 1	Dalnij Tjulkas	282.20	4.89	-3.25	Korte et al. (2005)
ru 1	Dalnij Tjulkas	282.20	4.15	-3.57	Korte et al. (2005)
ru 2	Dalnij Tjulkas	282.10	4.21	-3.22	Korte et al. (2005)
ru 3	Dalnij Tjulkas	281.90	3.12	-3.26	Korte et al. (2005)
ru 4	Dalnij Tjulkas	281.90	3.50	-3.43	Korte et al. (2005)
ru 4	Dalnij Tjulkas	281.90	4.26	-2.85	Korte et al. (2005)
RKI5-1	Alegozovo	272.00	4.77	-1.58	Grossman et al. (2008)
RKI5-2	Alegozovo	272.00	4.90	-1.42	Grossman et al. (2008)
RKI5-3	Alegozovo	272.00	4.85	-1.44	Grossman et al. (2008)
RKI5-4	Alegozovo	272.00	4.86	-1.41	Grossman et al. (2008)
RSS7-1	Sterlitamak	288.00	5.65	-0.90	Grossman et al. (2008)
RSS7-3	Sterlitamak	288.00	5.63	-0.81	Grossman et al. (2008)
RST27-1	Sterlitamak	291.00	5.11	-2.14	Grossman et al. (2008)
RST27-2	Sterlitamak	291.00	5.26	-2.18	Grossman et al. (2008)
RST27-3	Sterlitamak	291.00	5.22	-2.25	Grossman et al. (2008)
RST27-4	Sterlitamak	291.00	5.20	-2.12	Grossman et al. (2008)
RST27B-1	Sterlitamak	291.00	5.30	-2.20	Grossman et al. (2008)
RST27B-2	Sterlitamak	291.00	5.23	-2.18	Grossman et al. (2008)
RST27B-3	Sterlitamak	291.00	5.05	-2.11	Grossman et al. (2008)
RST27B-4	Sterlitamak	291.00	5.28	-2.17	Grossman et al. (2008)
RST29-1	Sterlitamak	291.00	5.47	-2.32	Grossman et al. (2008)
RST29-2	Sterlitamak	291.00	5.42	-2.34	Grossman et al. (2008)
RST29-3	Sterlitamak	291.00	5.43	-2.23	Grossman et al. (2008)
RST29-4	Sterlitamak	291.00	5.37	-2.11	Grossman et al. (2008)
RAK15-1	Sterlitamak	297.00	3.80	-1.41	Grossman et al. (2008)
RAK15-2	Sterlitamak	297.00	3.85	-1.35	Grossman et al. (2008)
RAK15-3	Sterlitamak	297.00	3.81	-1.37	Grossman et al. (2008)
RAK32-1	Sterlitamak	297.00	5.90	-1.72	Grossman et al. (2008)
RAK32-3	Sterlitamak	297.00	6.00	-1.82	Grossman et al. (2008)
RAK32-3	Sterlitamak	297.00	5.95	-1.64	Grossman et al. (2008)
RAK32-4	Sterlitamak	297.00	5.86	-1.83	Grossman et al. (2008)
RAK34-1	Sterlitamak	297.00	5.56	-1.79	Grossman et al. (2008)
RAK34-2	Sterlitamak	297.00	5.49	-1.76	Grossman et al. (2008)
RAK34-3	Sterlitamak	297.00	5.45	-1.77	Grossman et al. (2008)
RAK34-4	Sterlitamak	297.00	5.52	-1.63	Grossman et al. (2008)
RAK38-1	Sterlitamak	297.00	5.29	-1.94	Grossman et al. (2008)
RAK38-2	Sterlitamak	297.00	5.30	-2.08	Grossman et al. (2008)
RAK38-3	Sterlitamak	297.00	5.32	-2.20	Grossman et al. (2008)
RAK38-4	Sterlitamak	297.00	5.39	-1.98	Grossman et al. (2008)
RAK38B-1	Sterlitamak	297.00	5.20	-2.05	Grossman et al. (2008)
RAK38B-2	Sterlitamak	297.00	5.04	-2.01	Grossman et al. (2008)
RAK38B-3	Sterlitamak	297.00	5.27	-1.78	Grossman et al. (2008)
RAK38B-4	Sterlitamak	297.00	5.15	-1.76	Grossman et al. (2008)
RAK27-1	Sterlitamak	297.00	3.72	-2.52	Grossman et al. (2008)
RAK27-2	Sterlitamak	297.00	4.34	-2.21	Grossman et al. (2008)
RAK27-3	Sterlitamak	297.00	4.56	-2.17	Grossman et al. (2008)

1. (continued)

Specimen	Location	Age (GTS 04)	$\delta^{13}C$	$\delta^{18}O$	Reference
SS-1-96-1	Urals	274.30	6.40	1.01	Grossman et al. (2008)
SS-1-96-3	Urals	274.30	6.43	0.65	Grossman et al. (2008)
SS-1-96-4	Urals	274.30	6.69	0.31	Grossman et al. (2008)
SS6-96-12	Urals	274.20	6.32	0.44	Grossman et al. (2008)
SS6-96-13	Urals	274.20	6.52	0.31	Grossman et al. (2008)
SS6-96-14	Urals	274.20	5.72	0.51	Grossman et al. (2008)
SS6-96-15	Urals	274.20	6.53	0.26	Grossman et al. (2008)
SS6-96-16	Urals	274.20	5.85	0.02	Grossman et al. (2008)
SS7-96-5	Urals	274.30	4.83	-1.27	Grossman et al. (2008)
SS6-96-6	Urals	274.20	5.79	0.12	Grossman et al. (2008)
SS6-96-7	Urals	274.20	5.51	0.17	Grossman et al. (2008)
SS6-96-8	Urals	274.20	5.89	-0.23	Grossman et al. (2008)
SS6-96-9	Urals	274.20	5.97	-0.26	Grossman et al. (2008)
SS6-96-10	Urals	274.20	5.55	-0.34	Grossman et al. (2008)
SQ2-96-4	Urals	274.60	4.92	0.11	Grossman et al. (2008)
Ru-13-NL-1	Russia	269.00	3.34	0.67	Popp (1986)
Ru-14-1-NL-1	Russia	269.00	3.13	0.81	Popp (1986)
Ru-14-2-NL-1	Russia	269.00	3.41	-0.75	Popp (1986)
Ru-15-NL-1	Russia	269.00	3.35	0.95	Popp (1986)
Ru-16-NL-1	Russia	269.00	3.00	0.88	Popp (1986)
Ru-17-NL-1	Russia	269.00	3.88	1.48	Popp (1986)

2. Previously published North American brachiopod data

Specimen	Location	Age (GTS 04)	$\delta^{13}C$	$\delta^{18}O$	Reference
TXP001	Texas	272.00	2.86	-1.04	Grossman et al. (2008)
TXP002	Texas	272.00	3.10	-2.89	Grossman et al. (2008)
TXP003	Texas	272.00	4.63	-2.61	Grossman et al. (2008)
TXP004	Texas	272.00	3.72	-2.62	Grossman et al. (2008)
TXP005	Texas	272.00	3.90	-2.42	Grossman et al. (2008)
TXP006	Texas	272.00	4.12	-3.16	Grossman et al. (2008)
TXP007	Texas	272.00	4.25	-2.35	Grossman et al. (2008)
TXP008	Texas	272.00	3.96	-2.55	Grossman et al. (2008)
TXP074	Texas	275.00	1.90	-2.52	Grossman et al. (2008)
TXP077	Texas	275.00	2.25	-2.03	Grossman et al. (2008)
TXP065	Texas	284.00	5.84	-2.93	Grossman et al. (2008)
TXP023	Texas	295.00	3.17	-4.22	Grossman et al. (2008)
TXP023	Texas	295.00	3.17	-4.22	Grossman et al. (2008)
TXP024	Texas	295.00	5.73	-2.96	Grossman et al. (2008)
TXP025	Texas	295.00	5.76	-2.89	Grossman et al. (2008)
TXP028	Texas	295.00	3.27	-3.68	Grossman et al. (2008)
TXP068	Texas	295.00	5.47	-3.52	Grossman et al. (2008)
TXP052	Texas	296.00	5.07	-3.03	Grossman et al. (2008)
TXP053	Texas	296.00	5.38	-3.89	Grossman et al. (2008)
TXP012	Texas	296.50	5.60	-3.37	Grossman et al. (2008)
TXP013	Texas	296.50	5.38	-3.22	Grossman et al. (2008)
TXP014	Texas	296.50	4.85	-3.49	Grossman et al. (2008)
TXP054	Texas	296.50	5.64	-2.92	Grossman et al. (2008)
TXP057	Texas	296.50	4.54	-3.36	Grossman et al. (2008)
TXP018	Texas	297.00	4.18	-3.28	Grossman et al. (2008)
TXP020	Texas	297.00	2.39	-3.57	Grossman et al. (2008)

3. Non-Uralian data from Korte (2005) - all "bad" samples removed

Specimen	Location	Age (STD 02)	$\delta^{13}C$	$\delta^{18}O$
44403	Kansas	295.81	4.86	-1.37
36222	Kansas	295.42	4.87	-1.60
sb TG1 4.8-5.5	Svalbard	295.00	3.67	-2.33
bj Teltvika	Bjørnøya	292.00	3.70	-1.91
sb Nor 4	Svalbard	284.00	4.24	-1.84
bj HAM 1 16	Bjørnøya	281.75	3.41	-3.45
Roc 11	Sicily, Italy	276.00	3.95	-2.98
SC 27	Texas	273.91	4.35	-2.16
SC 30	Texas	273.83	3.29	-1.25

4. Running oxygen and carbon isotope means from **ALL** Korte et al. (2005) brachiopod data (5 Ma windows, 2 Ma steps)

Age (STD 02)	$\delta^{18}O$	$\delta^{13}C$
295.5	-0.94	4.45
293.5	-0.95	4.35
291.5	-0.70	4.08
289.5	-1.52	4.27
287.5	-2.06	4.30
285.5	-2.37	4.27
283.5	-3.01	4.01
281.5	-3.29	3.93
279.5	-3.25	3.57
277.5	-2.98	3.95
275.5	-2.13	3.86
273.5	-2.09	3.41
271.5	-2.26	3.50
269.5	-2.50	3.75
267.5	-2.25	4.56
265.5	-2.22	4.97
263.5	-2.44	4.76
261.5	-2.66	4.32
259.5	-2.82	4.03
257.5	-2.97	3.92
255.5	-3.03	3.98
253.5	-3.11	3.43
251.5	-3.04	3.25

APPENDIX D
ONLINE RESOURCES

As a supplement to the materials found within this thesis, some resources have been made available online at the website http://jordan.noret.info/research/2009/undergrad. This website will exist for as long as possible (likely forever) in order to make these resources available for readers of this thesis, as well as future researchers. Outlined below are the resources that can be found on this website. Efforts will be taken to convert these resources if the file formats become obsolete.

1. **Full-Resolution Specimen Image Repository**
   This repository makes available the full-resolution images of the specimens shown in Appendix B of this thesis: microscope photography maps, PL photos, CL photos, and sampling maps.

2. **Specimen Notes and Data Spreadsheet**
   This is the original spreadsheet used to make Appendix C of this thesis. It contains notes about the specimens and the data collected from them.

3. **Full-sized Data Plots**
   This file contains the full-sized versions of Figures 7 and 8 from this thesis.

4. **Raw Isotope Data**
   These are the original spreadsheets that contain the raw isotope data collected from each specimen. These are made available to allow for the utmost transparency in this project.

5. **Google Earth File (.kmz)**
   This file can be loaded into Google Earth to display the specimen localities along with information on the specimens and photographs of the localities.

CONTACT INFORMATION

Name:	Jordan Noret
Professional Address:	c/o Dr. Ethan Grossman Department of Geology and Geophysics MS 3115 Texas A&M University College Station, TX 77843
Email Address:	jordannoret@gmail.com
Education:	B.S., Geology and Environmental Geoscience Texas A&M University, December 2008 Accepted into Ph.D. program at Southern Methodist University, January 2009